HHS Public Access

Author manuscript

J Comp Neurol. Author manuscript; available in PMC 2021 October 01.

Published in final edited form as:

J Comp Neurol. 2020 October ; 528(14): 2283–2307. doi:10.1002/cne.24893.

Straying from the flatfish retinal plan: cone photoreceptor patterning in the common sole (*Solea solea*) and the Senegalese sole (*Solea senegalensis*)

Sara Frau[1], **Iñigo Novales Flamarique**[2,3,*], **Patrick W. Keeley**[4], **Benjamin E. Reese**[4,5], **José A. Muñoz Cueto**[1]

[1]Department of Biology, Faculty of Marine and Environmental Sciences, University of Cádiz, The European University of the Seas (SEA-EU), Campus Rio San Pedro, E-11510 Puerto Real, Spain.

[2]Department of Biological Sciences, Simon Fraser University, Burnaby, British Columbia, V5A 1S6, Canada.

[3]Department of Biology, University of Victoria, Victoria, British Columbia, V8W 2Y2, Canada.

[4]Neuroscience Research Institute, University of California Santa Barbara, Santa Barbara, California, United States of America.

[5]Department of Psychological and Brain Sciences, University of California Santa Barbara, Santa Barbara, California, United States of America.

Abstract

The retinas of non-mammalian vertebrates have cone photoreceptor mosaics that are often organized as highly patterned lattice-like distributions. In fishes, the two main lattice-like patterns are composed of double cones and single cones that are either assembled as interdigitized squares or as alternating rows. The functional significance of such orderly patterning is unknown. Here, the cone mosaics in two species of Soleidae flatfishes, the common sole and the Senegalese sole, were characterized and compared to those from other fishes to explore variability in cone patterning and how it may relate to visual function..The cone mosaics of the common sole and the Senegalese sole consisted of single, double and triple cones in formations that differed from the traditional square mosaic pattern reported for other flatfishes in that no evidence of higher order periodicity was present. Furthermore, mean regularity indices for single and double cones were conspicuously lower than those of other fishes with “typical” square and row mosaics, but comparable to those of goldfish, a species with lattice-like periodicity in its cone mosaic. Opsin transcripts detected by qPCR (*sws1*, *sws2*, *rh2.3*, *rh2.4*, *lws*, and *rh1*) were uniformly expressed

*Correspondence to: Iñigo Novales Flamarique, inigo@sfu.ca;.

AUTHOR CONTRIBUTIONS

SF and INF performed the experiments and their analyses. SF and INF drafted the figures and INF wrote the article. PK and BR provided the Matlab software and guided its use. INF and JAMC conceived the study. All authors reviewed and approved the manuscript.

CONFLICT OF INTEREST

The authors declare no conflict of interest

DATA AVAILABILITY STATEMENT

The data that support the findings of this study are available from the corresponding author (INF) upon reasonable request.

across the retina of the common sole but, in the Senegalese sole, *sws2*, *rh2.4* and *rh1* were more prevalent in the dorsal retina. Microspectrophotometry revealed five visual pigments in the retina of the common sole [S(472), M(523), M(536), L(559) and rod(511)] corresponding to the repertoire of transcripts quantified except for *sws1*. Overall, these results indicate a loss of cone mosaic patterning in species that are primarily nocturnal or dwell in low light environments as is the case for the common sole and the Senegalese sole. The corollary is that lattice-like patterning of the cone mosaic may improve visual acuity. Ecological and physiological correlates derived from observations across multiple fish taxa that live in low light environments and do not possess lattice-like cone mosaics are congruent with this claim.

Graphical Abstract

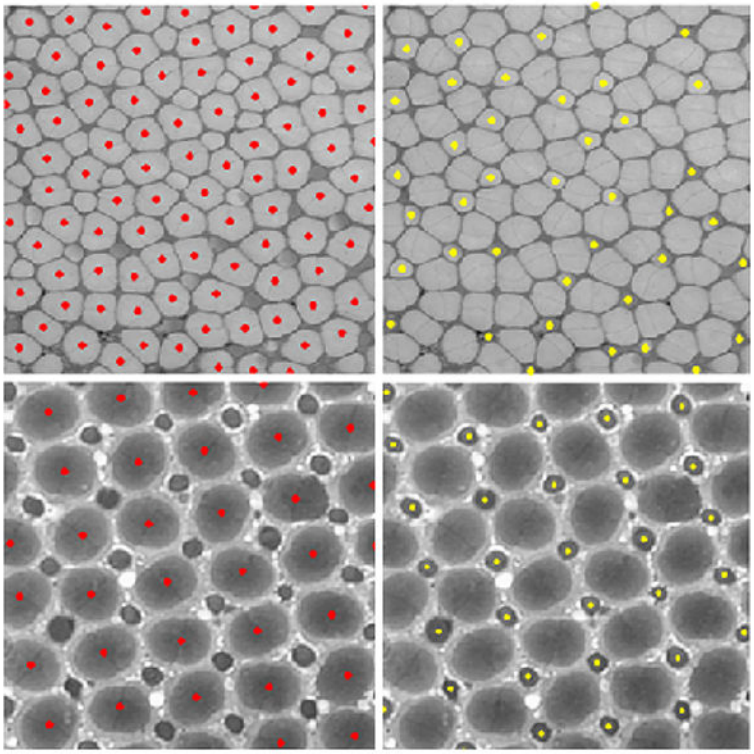

The retinas of many fishes are characterized by single and double cones that are organized into lattice-like formations. The functional significance of such cone mosaic periodicity is unknown. Unlike other flatfishes, the common sole and the Senegalese sole lack lattice-like organization of their cone mosaics. These findings suggest that square mosaics improve visual acuity and that lattice-like organization is lost as fish become nocturnal or live in low light environments.

Keywords

photoreceptor; retina; cone distributions; visual pigment; opsin transcript

INTRODUCTION

The retinas of vertebrates possess two main morphological types of photoreceptors: rods and cones. These are highly specialized neurons with a soma that projects an axon terminal at the basal end, and a cilium, known as the outer segment, that extends at the apical end (Ebrey & Koutalos, 2001). The outer segment comprises stacks of lipid bilayers which contain the visual pigments that capture light to begin the process of phototransduction. Each visual pigment is a complex of a protein (opsin) and a chromophore (retinal, the aldehyde of vitamin A_1, or 3,4-dehydroretinal, the aldehyde of vitamin A_2; Bridges, 1972; Hárosi, 1994); the spectral phenotype of a photoreceptor is determined by the predominant visual pigment that it contains. There are six main families of vertebrate visual opsins, most sensitive to either ultraviolet (UV) light (*sws1*), short wavelength or blue light (*sws2*), middle wavelength or green light (*mws*, *rh1*, and *rh2*), or long wavelength or red light (*lws*) (Yokoyama, 2000). With few exceptions (Kojima et al., 1992; Hisatomi et al., 1999; Takahashi et al., 2001; Ma et al., 2001), rod photoreceptors express *rh1* opsins whereas the rest of the opsins are found in cone photoreceptors.

In contrast to placental mammals, whose retinas have only single cones, non-mammalian vertebrates have two predominant cone types: single and double cones (Lyall, 1957; Engström, 1963; Hárosi & Novales Flamarique, 2012). A single cone, viewed perpendicular to the optical axis, exhibits a circular profile in cross-section whereas a double cone, which consists of two cells apposed together sharing a double membrane partition, shows an elliptical profile throughout most of the inner segment. In the vast majority of fishes that have been examined, single and double cone mosaics form organized lattice-like patterns (Lyall, 1957; Engström 1963; Cheng & Novales Flamarique, 2007; Novales Flamarique et al., 2013), which is also the case in some lizards (Loew et al., 1996). The predominant mosaic is known as the square mosaic whereby double cones form the sides of the unit square and single cones are located in the middle of the square (at the hypothetical intersection of neighbouring double cone partitions) and, when present, at the corners (facing the neighbouring double cone partitions) (Engström, 1963; Cheng & Novales Flamarique, 2007). Another mosaic type is the row mosaic, as exemplified by the retina of the adult zebrafish (*Danio rerio*), where rows of single cones alternate with those of double cones (Fang et al., 2013; Suliman & Novales Flamarique, 2014). Some species, including atheriniforms (Reckel et al., 2001; Reckel & Melzer, 2003), osmerids (Reckel et al., 2003), and salmonid fishes (Beaudet et al., 1997; Cheng et al., 2006, Cheng & Novales Flamarique, 2007) exhibit variations of the square and row mosaics as a function of retinal location, and this includes pentagonal and hexagonal formations where five and six double cones, respectively, surround a single cone (Lyall, 1957; Reckel et al., 2001; Reckel & Melzer, 2003). The shapes of the double cones can also change along their lengths, as in salmonid fishes (Novales Flamarique, 2001; Cheng et al., 2006), though the relative orientation of partitions between adjacent double cones tends to remain the same throughout the inner segment permitting the identification of centre and corner cones in tangential sections of light-adapted retina (Novales Flamarique, 2001).

There are three notable, non-mutually exclusive exceptions to the above general arrangements of cones in the retinas of fishes. The first is found in some deep water

(bathypelagic) teleosts with non-tubular eyes (Wagner et al., 1998) and in some species of elasmobranchs (Lisney et al., 2012) and night-active eels (Heβ et al., 1998), which have rod dominated retinas with few, if any, cones. No lattice-like cone arrangements have been reported in these fish groups. The second comprises a diverse group of species that have grouped retinas, i.e., in which the cones (or rods) group into bundles shielded by crystal structures; these often act as "megareceptors" to improve sensitivity in low light environments (Francke et al., 2014). The third is found among anchovies where a variety of unusual polycone formations have been reported (Fineran & Nichol, 1978; Heβ et al., 2006). In some anchovy species, the cones are morphologically segregated in that continuous rows of two alternating types of single cone dominate the ventro-temporal retina whereas rows of triple cones and single cones are found in other parts of the retina (Heβ et al., 2006; Novales Flamarique, 2011; Kondrashev et al., 2012). Triple cones have also been reported in other fish species (Shand et al., 1999; Miyazaki et al., 2002; Reckel & Melzer 2003; Fritsch et al., 2017) but, in these, the morphology is different from that found in anchovies and they constitute less than 1% of the cone population (though the triple cone can be dominant where found at highest density, Miyazaki et al., 2002; Fritsch et al., 2017). These three exceptions appear to have evolved for life in darkness or in very low light conditions, where maximum sensitivity is achieved by an almost rod exclusive retina (deep water fishes, Wagner et al., 1998; night-active eels, Heβ et al., 1998), and for polarization vision, at least in part, in the case of anchovies (Novales Flamarique, 2017, 2019).

Among fishes that experience photopic or mesopic environments, adult flatfishes have some of the most striking, well patterned square mosaics (Evans & Fernald, 1993; Iwanicki et al., 2017). These fishes undergo arguably the most pronounced metamorphosis among vertebrates starting with a bilaterally symmetric larva and terminating in a laterally compressed juvenile with both eyes on the same side of the body (Bao et al., 2011). In the larva of the winter flounder, *Pseudopleuronectes americanus*, and of the Atlantic halibut, *Hippoglossus hippoglossus*, only single cones have been reported prior to metamorphosis (Evans & Fernald, 1993; Forsell et al., 2001; Helvik et al., 2001a). During metamorphosis, some single cones appear to coalesce forming the double cones that are part of the square mosaic characteristic of the post-metamorphic retina (Hoke et al., 2006). The latter, adult-type mosaic is characterized by an almost complete absence of single corner cones and variable numbers of opsins and visual pigments, depending on the species examined.

Four cone opsin (*sws1*, *sws2*, *rh2* and *lws*) and one rod opsin (*rh1*) transcripts have been detected by *in-situ* hybridization during retinal development of the Atlantic halibut (Helvik et al., 2001a) and the winter flounder (Hoke et al., 2006). Microspectrophotometry measurements from winter flounder found only one middle wavelength (M) sensitive visual pigment prior to metamorphosis whereas the post-metamorphic retina had three cone visual pigments and one rod visual pigment (Evans et al., 1993), a finding in line with *in-situ* hybridization results (Hoke et al., 2006). The single cones contained a short wavelength sensitive (S) visual pigment, and the double cones were either equal (M/M) or unequal (M/L), containing an M or a long wavelength (L) sensitive visual pigment (Evans et al., 1993). In Atlantic halibut, the four cone opsin transcripts were detected prior to metamorphosis (Helvik et al., 2001a) and, post metamorphosis, the single cones express an *sws2* opsin transcript whereas the double cones express *rh2* or *lws*, being equal (M/M) or

unequal (M/L) members (Helvik et al., 2001b). More recently, microspectrophotometry studies on the barfin flounder, *Verasper moseri* (Kasagi et al., 2015), and the starry flounder, *Platichthys stellatus* (Iwaniki et al., 2017), have shown six and seven cone visual pigments, respectively, and one rod visual pigment following metamorphosis. In the starry flounder, single S cones and unequal (M/L) double cones co-express opsins and undergo opsin switches as they grow to the adult stage (Savelli et al., 2018). Opsin switches during metamorphosis are thought to occur in the winter flounder as well, as the visual pigment prior to metamorphosis is different from the repertoire present post metamorphosis (Hoke et al., 2006). In all the above species, overall cone density post metamorphosis is greater in the dorsal compared to the ventral retina, triple cones are extremely rare or absent and, at least in the young juvenile, there is variation in opsin expression with retinal location (Engström & Ahlbert, 1963; Evans & Fernald, 1993; Evans et al., 1993; Hoke et al., 2006; Helvik et al., 2001a,b; Iwanicki et al., 2017).

It is only in the case of one flatfish species, the common sole (*Solea solea*), that the cones were reported to be distributed "haphazardly" and "no assumption of a mosaic could be made" (Engström & Ahlbert, 1963). As evidence, the authors of this study provided a low magnification photograph of a section of unknown topographical origin and frequency plots of double cone orientations purportedly showing lack of a "common trend", though no statistical analyses were provided (Engström & Ahlbert, 1963). Nonetheless, these early observations were intriguing as the common sole shares similar habitat with many other flatfish species (Fernández-Zapico et al., 2017) and the ones that have been examined possess a square mosaic throughout the majority of the retina (Engström & Ahlbert, 1963). To assess whether the retinas of soles may indeed be exceptions to the general flatfish cone mosaic plan, we quantified the distribution of cone types and the patterning characteristics of the cone mosaic in the common sole and in a close relative, the Senegalese sole (*Solea senegalensis*). The Senegalese sole shares extensive habitat overlap with the common sole and the two species are morphologically similar (Vinagre et al, 2006). Because opsin expression changes with retinal location in early life stages of other flatfishes (Helvik et al., 2001a; Hoke et al., 2006; Savelli et al., 2018), we further quantified opsin transcripts in both species and measured visual pigments of the common sole. Patterning of the cone mosaic was also compared to that of additional fishes (starry flounder; coho salmon, *Oncorhynchus kisutch*; zebrafish, *Danio rerio*; and goldfish, *Carassius auratus*) to assess deviations from a range of mosaics reported in the literature. This study contributes to our understanding of cone mosaic organization in fishes and their potential functions.

MATERIALS AND METHODS

Fish and housing conditions

Fertilized eggs of common sole (*Solea solea*) were obtained from the Spanish Institute of Oceanography (Santander, Cantabria, Spain) during the spring reproductive season and carried to the University of Cádiz (Puerto Real, Spain). These were reared, along with locally collected Senegalese sole (*Solea senegalensis*) larvae, to the juvenile stage (180–250 days old; i.e, over 5 months after metamorphosis) in the Laboratorio de Cultivos Marinos (University of Cádiz). Animals of both sexes were kept in 500 l tanks with running seawater

at a constant temperature and salinity of 19±1 °C and 39 ppt, respectively, and experienced the natural daylight cycle. The mean weights and total lengths (± SD) of the fish used in the histology experiments were: 29 ± 17 g and 13 ± 2.8 cm (common sole; n= 8), and 25 ± 7.1 g and 12 ± 1.1 cm (Senegalese sole, n= 8). For the qPCR experiments, they were: 22 ± 6.8 g and 10 ± 2.6 cm (common sole; n= 8), and 18 ± 3.8 g and 8.9 ± 2.3 cm (Senegalese sole, n= 10). Common sole juveniles were transported from Cádiz to the University of Victoria Aquatic Facility where they were held in similar conditions (500 l outdoor tank with 18°C running water) prior to microspectrophotometry experiments at Simon Fraser University. The mean weight and total length (± SD) of the fish used for these experiments were: 23 ± 4.2 g and 12.7 ± 1.8 cm (n = 5). All holding and experimental procedures were approved by the Animal Care Committees of participating institutions which abide by the Animal Care Councils of Spain and Canada and by NIH guidelines. The Animal Care protocol numbers were: REGA ES11028000312 (University of Cádiz), 1126B-10 (Simon Fraser University), and 2013–005 (University of Victoria).

Histology

Individual fish were euthanized in the light adapted state after which the eyes were extracted, the lenses removed, and each eyecup immersed in primary fixative (2.5% glutaraldehyde, 1% paraformaldehyde in 0.08 M PBS, pH = 7.4) in a separate vial for the migrated or non-migrated eye. Following overnight fixation at 4°C, the retina was extracted from each eyecup, rinsed in 0.08 M PBS, and cut into four quadrants (ventro-temporal, VT; ventro-nasal, VN; dorso-nasal, DN; and dorso-temporal, DT). After a brief wash in distilled water, the tissue was dehydrated through a series of solutions of increasing ethanol concentration, infiltrated with mixtures of propylene oxide and EPON resin, and embedded in 100% EPON resin. Retinal blocks were cut tangentially or radially, in 2 μm steps, deposited on glass slides and stained with Richardson's solution (1:1 mixture of 1% Azure II in dH_2O and 1% Methylene blue in 1% NaB_4O_7) to reveal the cone mosaic and length of photoreceptors, respectively. Digital images of sections were acquired with an E-600 Nikon microscope equipped with a 60 × objective and magnification tourette (1.5x) and a DXM-100 digital camera. There were no differences in results between the migrated and non-migrated eye and, as such, they were pooled together for statistical analyses.

In addition to the flatfish retinas, sections were also obtained from previously embedded retinas of juvenile starry flounder (weight: 5.3 g, total length: 7.4 cm), coho salmon (weight: 13.1 g, total length: 11.6 cm), zebrafish (weight: 0.51g, total length: 3.9 cm) and goldfish (weight: 4.0 g, total length: 4.6 cm). These retinas had been prepared in the same way as the flatfish retinas used in the present study.

Morphometric analyses

Digital micrographs of tangential sections, each covering a 80 × 80 μm^2 area, at the level of largest double cone ellipsoid cross section, were analyzed with Photoshop (Adobe Systems) to extract the X-Y coordinates (centroids, assessed by eye) of every cone type (i.e., single, double and triple cone) in the field of view. The coordinates were then imported into a customized Matlab program that computed the Delaunay tessellation of the field, from which the nearest neighbour distance of each individual cell was determined, as was their

Voronoi domain area. Whereas the first analysis (nearest neighbour) is based on the relationship of each cell to only one of its neighbours, the second (Voronoi domain) analysis takes into account the relationship between each cell and all of its immediate neighbours by computing the area surrounding each cell that encloses the territory closer to that cell than to any of the neighbours (Reese & Keeley, 2015). Each analysis excluded “border cells”, i.e., those with uncertain nearest neighbour distances or Voronoi domain areas. In each case, the regularity index was defined as the mean divided by the standard deviation.

To assess whether the cone distributions analyzed had higher order (lattice-like) periodicity, a spatial auto-correlation analysis was carried out that examined the positioning of each cell with respect to all other cells across the mosaic. The Density Recovery Profile (DRP) was derived from each autocorrelogram (AC), providing a plot of the mean density of cells as a function of distance from each cell. The AC permits the detection of higher order patterning, even when it is subject to jitter (i.e., dispersion around periodic foci in the AC) and consequently less apparent in the mosaic itself. The DRP enables a measure of the exclusion zone surrounding each cell where other like-type cells are less likely to be found than at further distances (Reese & Keeley, 2015).

To further assess whether double cone arrangements were different from those expected in “typical” fish square mosaics, the orientation of double cones was examined for six samples per retinal quadrant at mid eccentricity per species. This was achieved by measuring the angle of the short axis of each double cone with respect to the horizontal (0–180° axis) in a 0.064 mm^2 area and determining the frequency within angular divisions comprising successive 30° increments (i.e., 1–30°, 31–60°, 61–90°, 91–120°, 121–150°, and 151–180°). This frequency distribution was compared by χ^2 test to an even distribution, the latter expected from a random double cone arrangement (Novales Flamarique & Hawryshyn, 1998). Lattice-like mosaics have frequency distributions that are grouped around two angles, corresponding to the two main orthogonal orientations of the double cone elliptical cross sections.

Cone densities over a 0.254 mm^2 area located at mid eccentricity for each sector of the retina were obtained from tangential sections showing mosaics at the level of greatest double cone ellipsoid area (n=8). The surface area of single and double cones (mean of 10 cones from each sector per retina) was derived by tracing the perimeter of each cell using Simple PCI software (Nikon). From these measures, cone packing was computed as the product of cone density and mean surface area for single and double cones divided by the retinal area analyzed in each sampled field, and expressed as a percentage.

Statistical analyses to assess differences in mosaic regularity, cone density and packing between retinal sectors were based on ANOVA with post-hoc grouping tests (Student-Newman-Keuls, Tukey HSD) evaluated at $\alpha = 0.05$ level of significance.

Microspectrophotometry

This analysis was restricted to retinas from common sole juveniles as live Senegalese sole could not be transported from Cádiz (Spain) to Canada where the microspectrophotometer is located due to import restrictions. Individual fish were dark adapted for 6 hours, following

which the fish was euthanized, one eye enucleated and the retina extracted and cut into dorsal and ventral halves under infrared illumination. Small pieces of retina were teased apart and prepared for viewing with the dichroic microspectrophotometer (DMSP) as per previous studies (Hárosi, 1987; Novales Flamarique & Hárosi, 2000, 2002). The DMSP is a computer-controlled, wavelength-scanning, single-beam photometer that simultaneously records average and polarized transmitted light fluxes through microscopic samples (Hárosi, 1987; Novales Flamarique & Hárosi, 2002). The DMSP was equipped with ultrafluar (Zeiss) objectives: 32/0.4 for the condenser and 100/1.20 for the objective. With the aid of reference measurements recorded through cell-free areas, individual photoreceptor outer segments were illuminated sideways with a measuring beam of rectangular cross section of ca. 2 × 0.6 μm. Absolute absorbance spectra were computed in 2 nm increments from the obtained transmittances (each spectrum consisted of an average of 8 scans). The solid spectra (fits) were derived from experimental data by Fourier filtering (Hárosi, 1987). Similar recordings were carried out for the migrated and non-migrated eye, which gave similar spectra, and the results were thus pooled together for statistical analyses.

Reverse transcriptase quantitative polymerase chain reaction (RT-qPCR)

Each fish was dark adapted for at least 1 hr before euthanasia following which both eyes were removed under infrared illumination, the lenses extracted, and each retina cut into the same four quadrants analyzed for histology (i.e., VT, VN, DT, DN). Quadrants from the migrated and non-migrated eye were placed into individual 1.5 ml Eppendorf tubes, immediately frozen in liquid nitrogen and stored at −80° C until processing.

RNA from each sample was extracted using the TRIsure Reagent® (Bioline). One μg of total RNA was reverse transcribed into cDNA (20 μl final volume) using the QuantiTect Reverse Transcription Kit (Qiagen). Specific primers for the various opsins in the common sole and the Senegalese sole were designed from an analysis of published sequences found in SoleaDB (Benzekri et al., 2014) and GenBank [https://www.ncbi.nlm.nih.gov/genbank] using primer3 v 0.4.0 software (Whitehead Institute for Biomedical Research). The identities of the opsin sequences were confirmed by BLAST [http://blast.ncbi.nml.nih.gov/Blast.cgi]. The opsins analyzed were: ultraviolet (*sws1*), short wavelength (*sws2*), middle wavelength (*rh2.3*, *rh2.4*), and long wavelength (*lws*) cone opsins, and rod opsin (*rh1*) (Tables 1,2). Percent similarity between full opsin sequences was obtained using Clustal W software.

RT-qPCR was performed in a Bio-Rad CFX96 Touch detection system (Bio-Rad) using SYBRPremix Ex TaqII (Tli RnaseH Plus, Takara Bio). A temperature gradient was carried out for each of the primers to determine the optimal temperature for PCR. Standard curves were also generated for each gene using 10-fold serial dilutions of cDNA. All calibration curves showed slopes close to −3.32 and efficiencies around 100%. Thermal cycling conditions for the PCR were as follows: 1 min denaturation at 95°C, followed by 40 cycles of a 15 s denaturation step at 95°C and by 15 s of annealing, and 10 s of elongation at 65°C. Following amplification, a melting curve analysis was performed to confirm the specificity of each amplicon, the identity of which was verified by sequencing. Non-template controls were used as negative controls. The 18s ribosomal unit of common sole and Senegalese sole

were used as housekeeping genes (SoleaDB accession number solea_solea_v1.0_unigene18130 and Gene bank accession number EF126042.1, respectively). Each qPCR reaction comprised duplicates per opsin gene from each eye; the results were statistically the same between eyes and were thus pooled together for further analyses.

For a given opsin transcript, the ΔΔCt method (Livak & Schmittgen, 2001) was used to compute the fold difference in expression in a given quadrant with respect to that in the VN quadrant (calibrator). These ratios were analyzed by one way ANOVA followed by Student-Newman-Keuls and Tukey HSD post-hoc grouping tests with $\alpha = 0.05$.

RESULTS

Cone photoreceptor types and distributions

Both the common sole and the Senegalese sole had three morphological cone types: single, double, and triple (Fig. 1,2). The single cone had a circular profile in cross-section whereas double cones, consisting of two members apposed together sharing a double membrane partition, showed variable elliptical profiles in cross-section, from quasi-rectangular to quasi-circular (Fig. 1,2). Triple cones were made up of three cells that, together, exhibited polygonal profiles in cross-section, with the shape often approximating a heptagon (Fig. 1e,2d). Single cones occurred alone, surrounded by double cones (and the occasional triple cones), or in groups consisting of up to 5 cells (Fig. 1b,g,2d). In tangential sections, single cones were surrounded by four to nine double cones (Fig. 1a,c,g,2a,g). In radial sections, two morphological types of single cones and double cones could be distinguished based on the shape of the ellipsoid and the double membrane partition, respectively (Fig. 3). Some single cones had a “pear shaped” inner segment whereas others were more streamlined and their inner segments reached further toward the retinal pigment epithelium (Fig. 3c,d). Among double cones, some appeared to consist of morphologically “equal” members, sharing a straight partition, whereas others were unequal members sharing a partition that was bent in the upper half of the inner segment (Fig. 3a,c). A comparison of 5 doubles from each category measured during microspectrophotometric recordings suggested that the outer segments of those with straight partitions were longer (mean ± SD: 9.9 ± 0.79 μm) than those from double cones with bent partitions (7.2 ± 1.6 μm; ANOVA $F_{1,8} = 10.998$, $p = 0.011$). In general, all cone types were larger in the central retina and decreased in size toward the periphery (Fig. 3).

A statistical analysis at mid eccentricity for the four retinal quadrants of both species showed that double cone density was greater in the ventral compared to the dorsal retina of the common sole (Fig. 4a; ANOVA $F_{3,28} = 12.48$, $p<0.001$), but not (at the limit of 5% significance) in the Senegalese sole (Fig. 4b; ANOVA $F_{3,28} = 2.95$, $p = 0.05$). This was primarily due to the smaller size of cells in the ventral retina (Fig. 1,2). All other variables examined [single cone density, double cone to single cone (d/s) ratio, and cone packing] were the same between quadrants for both species ($p > 0.05$; Fig. 4c–h). For both soles, triple cone density was greatest in the dorso-temporal quadrant (Fig. 1a) ranging from 2.3–3.7% of the cone population and lower (1.6–2.1%) in more peripheral areas of the dorsal

retina (Fig. 2d). Triple cone density in other retinal areas constituted less than 1% of the cone population.

Autocorrelation and Density Recovery Profile analyses

The autocorrelograms (AC) for a variety of Senegalese sole mosaics (Fig. 5a,d,g,j,m,p,s,v), which are representative of both *Solea* species (Fig. 1,2), revealed a lack of periodicity in the distributions of double cones (Fig. 5b, h,n,t) or single cones (Fig. 5e,k,q,w), as was apparent from examination by eye. The density recovery profile (DRP) derived from these ACs confirmed an absence of higher order periodicity, showing only a region surrounding the origin where the presence of like-type cones was absent. The size of this "exclusion zone" for the double cones (Fig. 5c,i,o,u) approximated the mean size of the ellipse axes of double cones themselves (6.8 μm) whereas it was slightly larger for the single cones (Fig. 5f,l,r,x), reflecting the greater distance between adjacent single cones due to the intervening presence of double cones and, when present, triple cones. In short, despite the lack of higher order patterning, the minimal spacing between either cone type appeared to be entirely accounted by the close packing of these cones and their interdigitated organization. Where such organization broke down, characterized by single cones infrequently coming in proximity of one another, ERs were as expected lower, approximating the diameter of the single cones themselves (e.g., Fig. 5v,w,x).

When the same analysis was performed on mosaics from other teleosts, the resulting AC plots, by contrast, showed a variety of lattice-like arrangements with different degrees of jitter (Fig. 6). Such dispersion surrounding these foci in the ACs was greatest for the goldfish (Fig. 6z,c'). Following from the high packing of cells and the closer proximity of double cones to each other compared to single cones, the ER was consistently equal or larger for the single cones (Fig. 6f,l,r,x,d') in comparison with the double cones (Fig. 6c,i,o,u,a').

Regularity of cone mosaics

Regularity analyses of the *Solea* cone distributions shown in Figure 5 revealed that double cone mosaics (Fig. 7) were characterized by smaller mean nearest neighbour distances and Voronoi domain areas than their single cone counterparts (Fig. 8), as might have been expected from their higher relative densities (Fig. 4). The same trends were found when analyzing the retinas of fishes with higher order lattice-like mosaics (Fig. 9,10). In comparison to the two *Solea* species (Fig. 7,8), the regularity indices of starry flounder, coho salmon and zebrafish were consistently greater, as expected from the periodicity present in their mosaics. Surprisingly, the results for goldfish were more closely comparable to those from the *Solea* species, particularly for the single cones (Fig. 10u–y), despite the periodicity revealed in the ACs (Fig. 6b'–d').

These results from individual *Solea* mosaics (Fig. 7,8) agreed with the statistical trends as revealed from an analysis of eight retinas per flatfish species (Fig. 11). Furthermore, the nearest neighbour distances, Voronoi domain areas and their associated regularity indices were not statistically different for a given cone type between quadrants within and between species ($p > 0.05$; Fig.11 a–h). Overall, these analyses show that the mosaics of both *Solea* species were indistinguishable with respect to their intercellular spacing and patterning.

The orientation of double cones was only statistically similar to a uniform distribution in the dorso-temporal quadrant of both *Solea* species. This result indicates a random distribution as the number of double cones whose orientation fell within each successive 30° angular increment, from 0°−180° (Novales Flamarique & Hawryshyn, 1998), was not statistically different. For instance, the mosaic shown in Figure 5a gave the following statistics: χ^2(df=5) = 6.23, significance = 0.285. All other samples from the remaining quadrants had orientations of double cones that were different from random (χ^2 significance < 0.05). This was also the case for all the non-flatfish mosaics shown in Figure 6, with the exception of the goldfish, which had a random distribution [χ^2(df =5) = 3.00, significance = 0.7].

Visual pigments

Absorbance measurements from the outer segment of individual photoreceptors from five common sole revealed four cone visual pigments and one rod visual pigment (Fig. 12). The cone visual pigments consisted of one S, with maximum wavelength of absorbance (λ_{max}) ± SD at 472 ± 7 nm (n = 8) (Fig. 12a), two Ms with respective λ_{max} ± SD at 523 ± 6 nm (n = 36) (Fig. 12b) and 536 ± 4 (n = 37) (Fig. 12c), and one L peaking at 559 ± 11 nm (n = 5) (Fig. 12d). The rod visual pigment had λ_{max} ± SD at 511 ± 7 (n = 17) (Fig. 12e). No UV visual pigment was found, a result in common with the winter flounder (Evans et al., 1993) and larger (weight > 16 g) starry flounder (Savelli et al., 2018). The S visual pigment was confined to the single cones whereas the M and L visual pigments were present in the double cones, one per double cone member. Within the population of double cones measured, the majority were M/M pairs, either 523/523 (n = 14) or 536/536 (n = 35), with a minority of M/L pairs (523/559, n= 5). The M/M pairs were primarily found in larger double cones, often characterized by straight partitions, whereas the M/L pairs tended to be associated with smaller double cones. No triple cones were encountered in these experiments.

Opsin gene sequences and transcript quantification

The opsin repertoire of both sole species was numerically identical. Corresponding opsin sequences between species had percent similarity of 90.3 (*sws2*), 96.9 (*lws*), 97.1 (*sws1*), 97.2 (*rh2.4*), and 98.3 (*rh2.3* and *rh1*). Potential absorbance tuning substitutions were located at position 97 of the *sws1* gene, positions 269 and 292 of the *sws2* gene, position 49 of the *rh2.3* gene and position 116 of the lws gene (Table 3;Yokoyama, 2008). For the common sole, the ratio of opsin transcript with respect to the calibrator (VN sector) was not significantly different between quadrants, irrespective of opsin type (p > 0.05; Fig. 13). For the Senegalese sole, however, the DN quadrant had greater fold expression over the VN sector of *sws2* ($F_{1,2}$ = 5.6, p = 0.01), *rh2.4* ($F_{1,2}$ = 5.6, p = 0.01) and *rh1*($F_{1,2}$ = 4.7, p = 0.02) compared to the VT quadrant (Fig. 14) denoting overall greater expression of these transcripts in the dorsal retina. The remainder of the transcripts had the same expression across the retina (p > 0.05).

DISCUSSION

Unconventional mosaics in the retinas of two *Solea* flatfish species

Of over 822 species of flatfishes so far documented in the literature (Munroe, 2015), only 15 have had some part of the retina examined for cone mosaic organization (Engström &

Ahlbert, 1963; Evans & Fernald, 1993; Helvik et al., 2001b; Hoke et al, 2006; Matsuda et al., 2008; Hunt et al., 2015; Iwanicki et al., 2017). These species are all in the genus Pleuronectiformes, with 12 of them belonging to the family Pleuronectidae (European flounder, *Platichthys flesus*; lemon sole, *Microstomus kitt*; European plaice, *Pleuronectes platessa*; winter flounder, *Pseudopleuronectes americanus*; Atlantic halibut, *Hippoglossus hippoglossus*; common dab; *Limanda limanda*; American plaice, *Hippoglossoides platessoides*; marbled sole, *Pseudopleuronectes yokohamae*; pointhead flounder, *Cleisthenes pinetorum*; slime flounder, *Microstomus achne*; red halibut, *Hippoglossoides dubius*; starry flounder, *Platichthys stellatus*), one in the family Paralichthyidae (olive flounder, *Paralichthys olivaceus*), one in the family Botidae (crested flounder, *Lophonectes gallus*), and one in the family Soleidae (common sole, *Solea solea*). With the exception of the latter, the retinas of all others were reported to show a square mosaic with the basic unit consisting of four double cones surrounding a centre cone, and corner cones in restricted areas of the dorsal retina when present (Engström & Ahlbert, 1963; Matsuda et al., 2008; Iwanicki et al., 2017).

Our findings for the common sole and the Senegalese sole mark a pronounced departure from the highly ordered, lattice-like mosaics of other flatfishes examined. As opposed to a lattice made up of double and single centre cones in 2:1 ratio throughout most of the retina (Evans & Fernald, 1993; Iwanicki et al., 2017), the *Solea* species had single, double and triple cones in variable formations with a mean double to single cone ratio in the range 2.4–3.1 (Fig. 4). Compared to the starry flounder, a flatfish with a cone mosaic representative of other Pleuronectiforms, the common sole and Senegalese sole had single and double cone mosaics that were conspicuously less orderly. This was also the trend when comparing the *Solea* species to other non-flatfish species with square (coho salmon) and row (zebrafish) mosaics. It is only when comparing to goldfish, a bottom dwelling cyprinid, that the *Solea* mosaic showed a closer degree of irregularity. Indeed, previous studies deemed that the cone distributions of goldfish were less regular than those of non cyprinid teleosts, with single cones thought to be more regularly distributed than double cones (Marc & Sperling, 1976; Zaunreiter et al., 1991). The latter conclusion is not supported by our analysis (Fig. 6,9,10).

Our results indicate that the developmental processes that establish the lattice-like arrangements of cones in the other fish species studied here are absent in the two soles. All species examined had highly packed cone mosaics, where regularity is primarily determined by the constraining effect of this packing, coupled with a periodic organization when present. Because the cones of goldfish, a species with lattice-like organization, had regularity indices that were closer to those from the two *Solea* species, the increasing jitter in that periodicity (e.g., Fig. 6z,c') must be responsible for this reduction in regularity from all other fish species examined. Perhaps fishes that occupy new niches in low light environments lose their lattice-like organization, in turn reducing the regularity of their cone patterning.

Triple cones

In fishes where they have been documented, triple cones are found in greatest densities in the dorso-temporal retina, with numbers that can exceed all other cone types at their location

of maximal density (Shand et al., 1999; Miyazaki et al., 2002; Reckel & Melzer 2003; Fritsch et al., 2017). However, over the entire retina, triple cones constitute less than 1% of the cone population, except in anchovies, but in the latter triple cones do not resemble those in other fish species (Heβ et al., 2006; Novales Flamarique, 2011). The triple cone densities in the common sole and Senegalese sole exceeded 1% of the cone population in some areas of the dorsal retina, notably in the proximal centro-temporal region. Ventral areas tended to have triple cones that numbered less than 1% of the cone population. These results conform to the trends found in other fish species with triple cones (Fritsch et al., 2017). The functions of triple cones are unknown but their morphology allows for similar or greater cone packing in the retinas of the common sole and the Senegalese sole compared to the range found in other fish species (e.g., the salmonid fishes, Beaudet et al., 1997). This suggests a function in enhancing total photon catch (overall sensitivity) of retinal regions where they occur. Coincidently, triple cones have not been reported in foveas, which are areas associated with greatest spatial resolution (visual acuity).

Flatfish visual ecology and divergence from the lattice mosaic plan

Flatfishes inhabit a large range of habitats with multiple species occurring sympatrically in time (e.g., at different life history stages or as a function of daily or seasonal migrations) and space (e.g., as a function of depth and substrate type) (McCracken, 1963; Reum & Essington, 2011). In general, recently metamorphosed juveniles inhabit nursery areas that range from ~0.5–50 m in depth (McCracken, 1963; Gibson et al., 2002; Reum & Essington, 2011; Ryer et al., 2012). But even in rearing estuaries of less than 5 m in depth, there can be spatial segregation between younger and older juveniles (Gibson et al., 2011), as well as between species (Marchand, 1988; Vinagre et al., 2006, 2009), depending on slight differences in ecotype and predation pressure (Vinagre et al., 2009; Gibson et al., 2002; Ryer et al., 2012). As flatfishes grow, they expand their ranges into deeper waters, with different species seemingly favouring different depths (Sohn et al., 2016; Fernández-Zapico et al., 2017; Sobocinski et al., 2018; Rau et al., 2019) likely as a result of multiple factors including substrate type (often correlated with prey type, Vinagre et al., 2009; Perry et al., 1994; Fernández-Zapico et al., 2017; Rau et al. 2019), complexity of habitat structure (e.g., presence of large rocks, sponges, bryozoan colonies; Ryer et al., 2012), oxygen availability (Sobocinski et al., 2018), temperature (Perry et al., 1994; Vinagre et al., 2009; van Hal et al., 2016; Rau et al., 2019), salinity (Vinagre et al., 2009; Rau et al., 2019) and risk of predation (Hurst et al., 2007; Reum and Essington, 2011; Yeung and Yang, 2018). Different flatfish species also vary in their displacement behaviour (remaining primarily on the bottom or frequently swimming in the water column; Hurst et al., 2007; Vollen & Albert, 2008), camouflage capabilities (active mimicry by changing skin pattern or digging into the substrate; Ryer et al., 2004, 2008), and prey spectrum (consuming more demersal species, like amphipods or polychaete worms, or pelagic species, such as mysids, euphausids and fish; Martell & NcClelland, 1994). These differences in life history strategies and behaviours presumably evolved in parallel with sensory systems that favoured success in critical ecological tasks, such as prey and predator detection, in one or multiple environments. The stark contrast between the cone mosaics of the *Solea* species examined and the rest of the flatfishes reported in the literature raises questions about the advantages of cone mosaic patterning, specifically lattice-like periodicity, in visual function.

As opposed to the open coastal waters inhabited by the majority of flatfishes whose retinas have been examined, often characterized by wide spectrum (λ range ~335–800 nm) light transmission in surface waters (~ upper 5 m) and narrowing to middle wavelengths (λ_{max} transmission around 560–570 nm) with depth (Savelli et al., 2018), the *Solea* species studied here favour estuaries with river discharge where turbidity can be high (Marchand, 1988) and light penetration limited (Jerlov, 1976). Furthermore, both species are primarily nocturnal after metamorphosis (Lagardère, 1987; Bayarri et al., 2004; Blanco-Vives et al., 2012). In such environments, image forming by any visual system would be challenging and the ability to detect detail (i.e., visual acuity) reduced. It appears that one of the main visual adaptations to life in such environments has been a loss of lattice-like periodicity in the cone mosaic since the number of visual pigment/opsin transcript types remains comparable in Soleidae with respect to other flatfish families (Pleuronectidae). Nonetheless the visual pigment repertoire may become reduced with growth as no UV visual pigment was found and L occurrence was minor among double cones; this is the trend reported for other flatfishes (Kasagi et al., 2015; Savelli et al., 2018). The retina may also become spectrally more homogeneous as the common sole examined by qPCR, which were slightly larger than the corresponding Senegalese sole, did not differ in fold expression per transcript. Further studies that examine earlier and later life stages and incorporate topographical cellular markers, such as riboprobes or antibodies, should be conducted to explore this topic.

Ecological studies have shown that both the common sole and the Senegalese sole feed on small, bottom dwelling invertebrates, with the common sole preferring amphipods and the Senegalese sole polychaete worms (Vinagre et al., 2006, 2009). It has further been shown that detection of prey is primarily olfactory driven whereas vision is favoured in predator detection (Maia et al., 2009). Thus, a cone mosaic without lattice-like structure, but with packing significantly greater than that found in other flatfish species (Fig. 4; Iwanicki et al., 2017), appears suitable for life in low light environments.

Insights into function of cone mosaic patterning

The evolution of mosaic structure of *Solea* flatfishes may provide insights into the functional significance of cone mosaic patterning. In particular, the function of the square mosaic (and the *raison d'être* of double cones) remains a mystery though several hypotheses have been proposed. These include increased overall sensitivity *via* enhanced cone packing (van der Meer, 1992), improved colour contrast (Fernald, 1981; van der Meer, 1992), a role in motion detection (Lyall, 1957; Ahlbert, 1973; Wagner, 1990; van der Meer, 1992) and in visual acuity (Engström, 1963). The retinas of the *Solea* species examined here demonstrate that superior packing can be achieved with less regularity compared to lattice-like mosaics, especially when the former combine a greater variety of irregular ellipsoidal cone cross-sections. Thus, the packing argument for enhanced sensitivity of a more regular mosaic does not apply. The other three hypotheses rely on correlations between cone mosaics and feeding behaviours (Lyall, 1957; Engström, 1963; Ahlbert, 1973) and, more recently, on observations that one or both members of double cones may be used for chromatic (colour vision) or achromatic (motion detection) tasks in various fish species (Orger & Baier, 2005; Pignatelli et al., 2010; Zukoshi et al., 2019). The dependence of these tasks on cone mosaic patterning, however, has not been established. A colour sensing system mediated by inputs

from a chromatically regular cone mosaic would, theoretically, improve colour contrast by sensing a background that does not change due to spectrally different cone inputs (at least for the brief duration of target detection). We argue that the same principle, based on homogenous sampling of target and background would also improve visual acuity.

Aside from the power of the dioptric apparatus and the density of photoreceptors and ganglion cells (Rossi & Roorda, 2010), visual acuity is also determined by other biological parameters that influence perceived contrast of the target against the background. High regularity of the cone mosaic coupled to similar regularity of spectral cone types would favour uniform sampling of the background and, we propose, the fine detection of edges. This is because colour and luminosity-based contrasts between various parts of the target and background would not be influenced by variable cone input to adjacent center-surround receptive fields that view the target and immediate background. If different regions of a target contour change in colour and/or luminosity contrast with respect to the background due to cone input inhomogeneity, smaller targets such as zooplankton could easily become distorted or blurred with the background, especially in a low light environment. This is because the sharpened detection of edges conferred by center-surround horizontal cell inhibition (Wagner, 1975) could be diminished if cone input is not uniform (i.e., spectrally regular). In addition, perception of detail within the target (prey or predator) may also be degraded if spatial resolution follows the Helmholtzian principle (Northmore et al., 2007) of one unstimulated receptive field in between stimulated receptive fields. This is because the less regular cone mosaic may not only lead to chromatically but also spatially variable receptive fields which could reduce the difference in activity between unstimulated and stimulated ones. It is interesting to note that the visual acuity of recently metamorphosed plaice and turbot (*Scophthalmus maximus*), two Pleuronectid flatfishes, is better (Neave, 1984) than that of goldfish of similar or larger size (Northmore & Dvorak, 1979) though the latter have larger lenses, the primary determinant of improved visual acuity with fish growth. In addition, in both Pleuronectid species investigated by Neave (1984), visual acuity reached a plateau during metamorphosis even though lens diameter continued to increase linearly throughout the study (and at a greater rate than the decrease in cone density). These results suggest that the appearance of double cones enhances visual acuity and that the extent of improvement is correlated to the degree of mosaic patterning.

Ecologically, high resolution of contours would be irrelevant to the detection of predators, which are bigger and cast a shadow over a large area of retina. In fishes, this would trigger the OFF response from the combined activity of many receptive fields whose primary input are cones tuned to the transmitted spectrum of downwelling light (Novales Flamarique & Wachowiak, 2015). The latter agrees well with the majority of cones being M type in the *Solea* species examined as middle wavelengths are preferentially transmitted in turbid coastal waters (Jerlov, 1976). Spectral sensitivity maxima derived from horizontal cell responses of isolated retinae from several species of adult Pleuronectid flatfishes peak in the range 518–544 nm (Matsuda et al., 2009).

Cone mosaic patterning across diverse fish taxa: ecophysiological correlations

The idea that lattice-like patterning of the cone mosaic should improve visual acuity is consistent with several related observations from different fish species. As per the results for the common sole, Senegalese sole, and goldfish, other species that inhabit turbid waters, such as the common white sucker, *Catostomus commersonii*, and multiple cyprinid fishes show irregular mosaics coupled with randomly oriented double cones (Zaunreiter et al., 1991; Novales Flamarique & Hawryshyn, 1998). Such bottom-dwelling species favour a combination of chemoreception and somatosensation for prey localization and, as adults, detect silhouettes of predators that attack from above. Catfishes, which also inhabit turbid environments and rely on non-visual cues for prey localization, have only single cones in their retinas (Douglas et al., 2002). The lack of double cones among catfishes is reminiscent of the flatfish retina prior to metamorphosis when visually-mediated prey detection capabilities are markedly reduced (compared to after metamorphosis, Evans & Fernald, 1993). These examples suggest that a lattice-like mosaic organization comprising double cones enhances visual performance of the animal, likely through a combination of improved visual acuity, colour contrast, and motion detection.

A large number of fishes with grouped retinae also do not exhibit cone mosaics with double cones. Instead, in these species, single cones or rods are grouped to form “megareceptors” whose primary function is to enhance overall sensitivity and, thus, luminosity based contrast (Francke et al., 2014). These fishes also dwell in very low light environments and generally do not rely on high acuity vision for prey localization. Among bathypelagic fishes, which often inhabit depths beyond 1000 m (considered to be the approximate maximum depth of light penetration in the ocean; Jerlov 1976), most have no cones and possess, instead, multi-banks of rods (Wagner et al., 1998). Such retinas are adapted for maximal sensitivity, not visual acuity. Among deep water fishes, some have tubular eyes with a fovea in which double cones appear in rows that are thought to mediate motion detection (Munk, 1977). The rest of the retina is dominated by groups of rods, with the occasional single and triple cones in parafoveal regions. Deep water fishes, with a lack of square mosaics, indirectly support a role for such a mosaic type in visual acuity and, perhaps, colour contrast.

At least one additional line of evidence suggests that cone mosaic periodicity should enhance visual acuity. The photoreceptors of many fishes that experience photopic light environments undergo retinomotor movements whereby cones and rods move in opposite directions with respect to the retinal pigment epithelium depending on time of day (Menger et al., 2005). As a result, during the day, cone outer segments are displaced vitreally with respect to those of rods, which are embedded in the retinal pigment epithelium. The exposed cones are arranged in a regular pattern, usually a square or a row, and mediate all aspects of photopic vision including colour discrimination and high spatial and temporal resolution. As light levels decrease toward scotopic conditions, cones move closer to the retinal pigment epithelium and mosaic regularity is lost (Reckel et al., 2003; Cheng et al., 2006). This is accompanied by a progressive dominance of rod activity, which are the photoreceptors associated with high sensitivity but low spatial and temporal resolution (Ebrey & Koutalos, 2001). As such, cone mosaic regularity diminishes as vision progresses toward a reduced state of visual acuity, colour contrast, and motion detection.

In summary, the loss of lattice-like structure and the associated decline in cone mosaic regularity of two Soleidae flatfish species, coupled with their nocturnal behaviour and reliance on non-visual sensory cues to detect small prey, suggests a function of cone mosaic patterning in visual acuity. In conjunction with published observations from other fish species spanning the range of photic habitats, our results support two main evolutionary trends associated with life in low light environments: loss of cone mosaic patterning and reduced cone visual pigment repertoire.

OTHER ACKNOWLEDGEMENTS

Thanks to Lisa Grebinsky for assistance with fish husbandry, experimentation and analyses.

Grant sponsors: Natural Sciences and Engineering Research Council of Canada (NSERC) grants RGPIN-2018-05722 and RGPAS-2018-522696 to INF; Spanish Ministry of Science, Innovation and Universities grants AGL2013-49027-C3-2-R and AGL2017-82582-C3-1-R to JAMC; National Institutes of Health grant EY-019968 to BER.

LITERATURE CITED

Ahlbert I-B. (1973). Ontogeny of double cones in the retina of perch fry (Perca fluviatilis, Teleostei). Acta Zoologica, 54, 241–254.

Bao B, Ke Z, Xing J, Peatman E, Liu Z, Xie C, … Ren D (2011). Proliferating cells in suborbital tissue drive eye migration in flatfish. Developmental Biology, 351, 200–207. [PubMed: 21195706]

Bayarri MJ, Muñoz-Cueto JA, López-Olmeda JF, Vera LM, Rol de Lama MA, Madrid JA, & Sánchez-Vázquez FJ (2004). Daily locomotor activity and melatonin rhythms in Senegal sole (Solea senegalensis). Physiology and Behavior, 81, 577–583. [PubMed: 15178150]

Beaudet L, Novales Flamarique I, & Hawryshyn CW (1997). Cone photoreceptor topography in the retina of sexually mature Pacific salmonid fishes. Journal of Comparative Neurology, 383, 49–59. [PubMed: 9184985]

Benzekri H, Armesto P, Cousin X, Rovira M, Crespo D, Merlo MA, & Manchado M (2014). De novo assembly, characterization and functional annotation of Senegalese sole (Solea senegalensis) and common sole (Solea solea) transcriptomes: integration in a database and design of a microarray. BMC Genomics, 15, 952. [PubMed: 25366320]

Blanco-Vives B, Aliaga-Guerrero M, Cañavate JP, García-Mateos G, Martín-Robles AJ, Herrera-Pérez P, Muñoz-Cueto JA, & Sánchez-Vázquez FJ (2012). Metamorphosis induces a light-dependent switch in Senegalese sole (Solea senegalensis) from diurnal to nocturnal behavior. Journal of Biological Rhythms, 27, 135–144. [PubMed: 22476774]

Bridges CDB (1972). The rhodopsin-porphyropsin visual system In Dartnall HJA (Ed.), Handbook of Sensory Physiology (pp. 417–480). Springer.

Cheng CL, & Novales Flamarique I (2007). Chromatic organization of cone photoreceptors in the retina of rainbow trout: single cones irreversibly switch from a UV (SWS1) to a blue (SWS2) light sensitive opsin during natural development. Journal of Experimental Biology, 210, 4123–4135. [PubMed: 18025012]

Cheng CL, Novales Flamarique I, Hárosi FI, Rickers-Haunerland J, & Haunerland NH (2006). Photoreceptor layer of salmonid fishes: transformation and loss of single cones in juvenile fish. Journal of Comparative Neurology, 495, 213–235. [PubMed: 16435286]

Douglas RH, Collin SP, & Corrigan J (2002). The eyes of suckermouth armoured catfish (Loricariidae, subfamily Hypostomus): pupil response, lenticular longitudinal spherical aberration and retinal topography. Journal of Experimental Biology, 205, 3425–3433. [PubMed: 12364396]

Ebrey T, & Koutalos Y (2001). Vertebrate photoreceptors. Progress in Retinal and Eye Research, 20, 49–91. [PubMed: 11070368]

Engström K (1963). Cone types and cone arrangements in teleost retinae. Acta Zoologica, 44, 179–243.

Engström K, & Ahlbert I-B (1963). Cone types and cone arrangements in the retina of some flatfishes. Acta Zoologica, 44, 119–129.

Evans BI, & Fernald RD (1993). Retinal transformation at metamorphosis in the winter flounder (Pseudopleuronectes americanus). Visual Neuroscience, 10, 1055–1064. [PubMed: 8257662]

Evans BI, Hárosi FI, & Fernald RD (1993). Photoreceptor spectral absorbance in larval and adult winter flounder. Visual Neuroscience, 10, 1065–1071. [PubMed: 8257663]

Fang W, Bonaffini S, Zou J, Wang X, Zhang C, Tsujimura T, Kawamura S, & Wei X (2013). Characterization of transgenic zebrafish lines that express GFP in the retina, pineal gland, olfactory bulb, hatching gland, and optic tectum. Gene Expression Patterns, 13, 1560–154.

Fernald RD (1981). Chromatic organization of a cichlid fish retina. Vision Research, 21, 1749–1753. [PubMed: 7336611]

Fernández-Zapico O, Punzón A, Serrano A, Landa J, Ruiz-Pico S, & Velasco F (2017). Environmental drivers of the distribution of the order Pleuronectiformes in the Northern Spanish Shelf. Journal of Sea Research, 130, 217–228.

Fineran BA, & Nicol JAC (1978). Studies of the photoreceptors of *Anchoa mitchilli* and *Anchoa hepsetus* Engraulidae with particular reference to the cones. Philosophical Transactions of the Royal Society of London B 283, 5–60.

Forsell J, Ekström P, Novales Flamarique I, & Holmqvist B (2001). Expression pattern of pineal UV- and green-like opsins in teleosts. Journal of Experimental Biology, 204, 2517–2525. [PubMed: 11511667]

Francke M, Kreysing M, Mack A, Engelmann J, Karl A, Makarov F, Guck J, Kolle M, Wolburg H, Pusch R, von der Emde G, Schuster S, Wagner H-J, & Reichenbach A (2014). Grouped retinae and tapetal cups in some teleostian fish: Occurrence, structure, and function. Progress in Retinal and Eye Research, 38, 43–69. [PubMed: 24157316]

Fritsch R, Collin SP, & Michiels NK (2017). Anatomical analysis of the retinal specializations to a crypto-benthic, micro-predatory lifestyle in the Mediterranean triplefin blenny *Tripterygion delaisi*. Frontiers in Neuroanatomy, 11, 122. [PubMed: 29311852]

Gibson RN, Burrows MT, & Robb L (2011). Field experiments on depth selection by juvenile plaice *Pleuronectes platessa*. Marine Ecology Progress Series, 430, 197–205.

Gibson RN, Robb L, Wennhage H, & Burrows MT (2002). Ontogenetic changes in depth distribution of juvenile flatfishes in relation to predation risk and temperature on a shallow-water nursery ground. Marine Ecology Progress Series, 229, 233–244.

Hárosi FI. (1987). Cynomolgus and rhesus monkey visual pigments. Application of Fourier transform smoothing and statistical techniques to the determination of spectral parameters. Journal of General Physiology, 89, 717–743. [PubMed: 3598558]

Hárosi FI. (1994). An analysis of two spectral properties of vertebrate visual pigments. Vision Research, 34, 1359–1367. [PubMed: 8023444]

Hárosi FI, & Novales Flamarique I (2012). Functional significance of the taper of vertebrate cone photoreceptors. Journal of General Physiology, 139, 159–187. [PubMed: 22250013]

Heβ M, Melzer RR, & Smola U (1998). The photoreceptors of Muraena helena and Ariosoma balearicum - a comparison of multiple bank retinae in anguilliform eels (Teleostei). Zoologischer Anzeiger, 237, 127–137.

Heβ M, Melzer RR, Eser R, & Smola U (2006). The structure of anchovy outer retinae (Engraulididae, Clupeiformes) — A comparative light- and electron-microscopic study using museum-stored material. Journal of Morphology, 267, 1356–1380. [PubMed: 17051549]

Helvik JV, Drivenes Ø, Harboe T, & Seo HC (2001a). Topography of different photoreceptor cell types in the larval retina of Atlantic halibut (Hippoglossus hippoglossus). Journal of Experimental Biology, 204, 2553–2559. [PubMed: 11511671]

Helvik JV, Drivennes Ø, Naess TH, Fjose A, & Seo H-C (2001b). Molecular cloning and characterization of five opsin genes from the marine flatfish Atlantic halibut (Hippoglossus hippoglossus). Visual Neuroscience,18, 767–780. [PubMed: 11925012]

Hisatomi O, Takahashi Y, Taniguchi Y, Tsukahara Y, & Tokunaga F (1999). Primary structure of a visual pigment in bullfrog green rods. FEBS Letters, 447, 44–48. [PubMed: 10218579]

Hoke KL, Evans BI, & Fernald RD (2006). Remodeling of the cone photoreceptor mosaic during metamorphosis of flounder (Pseudopleuronectes americanus). Brain Behaviour and Evolution, 68, 241–254.

Hunt DE, Rawlison NJF, Thomas GA, & Cobcroft JM (2015). Investigating photoreceptor densities, potential visual acuity, and cone mosaics of shallow water, temperate fish species. Vision Research, 111, 13–21. [PubMed: 25872175]

Hurst TP (2016). Shallow-water habitat use by Bering Sea flatfishes along the central Alaska Peninsula. Journal of Sea Research, 111, 37–46.

Hurst TP, Ryer CH, Ramsey JM, & Haines SA (2007). Divergent foraging strategies of three co-occurring north Pacific flatsfishes. Marine Biology, 151, 1087–1098.

Iwanicki TW, Novales Flamarique I, Ausió J, Morris E, & Taylor JS (2017). Fine tuning light sensitivity in the starry flounder (Platichthys stellatus) retina: regional variation in photoreceptor cell morphology and opsin gene expression. Journal of Comparative Neurology, 525, 2328–2342. [PubMed: 28295290]

Jerlov NG (1976). Marine Optics. 230 pp. Elsevier.

Kasagi S, Mizusawa K, Murakami N, Andoh T, Furufuji S, Kawamura S, & Takahashi A (2015). Molecular and functional characterization of opsins in barfin flounder (Verasper moseri). Gene, 556, 182–191. [PubMed: 25433330]

Kojima D, Okano T, Fukada Y, Shichida Y, Yoshizawa T, & Ebrey TG (1992). Cone visual pigments are present in gecko rod cells. Proceedings of the National Academy of Sciences of the USA, 89, 6841–6845. [PubMed: 1379723]

Kondrashev SL, Gnyubkina VP, Valentina P, & Zueva LV (2012). Structure and spectral sensitivity of photoreceptors of two anchovy species: *Engraulis japonicus* and *Engraulis encrasicolus*. Vision Research, 68, 19–27. [PubMed: 22819727]

Lagardère JP (1987). Feeding ecology and daily food consumption of common sole, *Solea vulgaris* Quensel, juveniles on the French Atlantic coast. Journal of Fish Biology, 30, 91–104.

Lisney TJ, Theiss SM, Collin SP, & Hart NS (2012). Vision in elasmobranchs and their relatives: 21st century advances. Journal of Fish Biology, 80, 2024–2054. [PubMed: 22497415]

Livak KJ, & Schmittgen TD (2001). Analysis of relative gene expression data using real-time quantitative PCR and the 2(-Delta Delta C(T)) Method. Methods, 25, 402–408. [PubMed: 11846609]

Loew ER, Govardovskii VI, Röhlich P, & Szél Á (1996). Microspectrophotometric and immunocytochemical identification of ultraviolet photoreceptors in geckos. Visual Neuroscience, 13, 247–256. [PubMed: 8737275]

Lyall AH (1957). Cone arrangements in teleost retinae. Quarterly Journal of Microscopial Science, 98, 189–201.

Ma J-X, Znoiko S, Othersen KL, Ryan JC, Das J, Isayama T, Kono M, Oprian DD, Corson DW, Cornwall C, Cameron DA, Hárosi FI, Makino CL, & Crouch RK (2001). A visual pigment expressed in both rod and cone photoreceptors. Neuron, 32, 451–461. [PubMed: 11709156]

Maia A, Vinagre C, & Cabral HN (2009). Impact of a predator in the foraging behaviour of *Solea senegalensis*. Journal of the Marine Biological Association of the United Kingdom, 89, 645–649.

Marc RE, & Sperling HG (1976). The chromatic organization of the goldfish cone mosaic. Vision Research, 16, 1211–1224. [PubMed: 1006992]

Marchand J (1988). Seasonal distribution, growth and ecological role of the juvenile sole, *Solea solea* L population in the Loire estuary, France. Journal of Fish Biology, 33, 229.

Martell DJ, & McClelland G (1994). Diets of sympatric flatfishes, *Hippoglossoides platessoides*, *Pleuronectes ferrugineus*, *Pleuronectes americanus*, from Sable Island Bank, Canada. Journal of Fish Biology, 44, 821–848.

Matsuda K, Torisawa S, Hiraishi T, & Yamamoto K (2009). Comparison of the color vision and spectral sensitivity of three flatfish species of different ecotypes, and application to selective fishing methods. Fisheries Science, 75, 35–42.

Matsuda K, Torisawa S, Hiraishi T, & Yamamoto K (2008). Comparison of visual acuity and visual axis of three flatfish species with different ecotypes. Fisheries Science, 74, 562–572.

McCracken FD (1963). Seasonal movements of the winter flounder, Pseudopleuronectes americanus (Walbaum), on the Atlantic coast. Journal of the Fisheries Research Board of Canada, 20, 551–586.

Menger GJ, Koke JR, & Cahill GM (2005). Diurnal and circadian retinomotor movements in zebrafish. Visual Neuroscience, 22, 203–209. [PubMed: 15935112]

Miyazaki T, Iwami T, Somiya H, & Meyer-Rochow VB (2002). Retinal topography of ganglion cells and putative UV-sensitive cones in two antarctic fishes: Pagothenia borchgrevinki and Trematomus bernacchii (Nototheniidae). Zoological Science, 19, 1223–1229. [PubMed: 12499665]

Munk O (1977). The visual cells and retinal tapetum of the foveate deep-sea fish Scopelosaurus Lepidus (Teleostei). Zoomorphologie, 87, 21–49.

Munroe TA (2015). Systematic diversity of Pleuronectiformes In Gibson RN, Nash RDM, Geffen AJ, van der Veer HW HW (Ed.), Flatfishes: Biology and Exploitation (pp. 74–166). John Wiley & Sons Inc.

Neave DA (1984). The development of visual acuity in larval plaice (Pleuronectes platessa L.) and turbot (Scophthalmus maximus L.). Journal of Experimental Marine Biology and Ecology, 78, 167–175.

Northmore DPM, & Dvorak CA (1979). Contrast sensitivity and acuity of the goldfish. Vision Research 19, 255–261. [PubMed: 442550]

Northmore DPM, Oh D-J, & Celenza MA (2007). Acuity and contrast sensitivity of the bluegill sunfish and how they change during optic nerve regeneration. Visual Neuroscience, 24, 319–331. [PubMed: 17822574]

Novales Flamarique I (2019). Swimming behaviour tunes fish polarization vision to double prey sighting distance. Scientific Reports, 9, 944. [PubMed: 30700806]

Novales Flamarique I (2017). A vertebrate retina with segregated colour and polarization sensitivity. Proceedings of the Royal Society B, 284, 20170759. [PubMed: 28878058]

Novales Flamarique I (2011). Unique photoreceptor arrangements in a fish with polarized light discrimination. Journal of Comparative Neurology, 519, 714–737. [PubMed: 21246551]

Novales Flamarique I (2001). Gradual and partial loss of corner cone-occupied area in the retina of rainbow trout. Vision Research, 41, 3073–3082. [PubMed: 11711133]

Novales Flamarique I, Cheng CL, Bergstrom C, & Reimchen TE (2013). Pronounced heritable variation and limited phenotypic plasticity in visual pigments and opsin expression of threespine stickleback photoreceptors. Journal of Experimental Biology, 216, 656–667. [PubMed: 23077162]

Novales Flamarique I, & Hárosi FI (2000). Photoreceptors, visual pigments, and ellipsosomes in the mummichog killifish, *Fundulus heteroclitus*: a microspectrophotometric and histological study. Visual Neuroscience, 17, 403–420. [PubMed: 10910108]

Novales Flamarique I, & Hárosi FI (2002). Visual pigments and dichroism of anchovy cones: a model system for polarization detection. Visual Neuroscience, 19, 467–473. [PubMed: 12511079]

Novales Flamarique I, & Hawryshyn CW (1998). The common white sucker: a fish with ultraviolet sensitivity that lacks polarization sensitivity. Journal of Comparative Physiology A, 182, 331–341.

Novales Flamarique I, & Wachowiak M (2016). Functional segregation of retinal ganglion cell projections to the optic tectum of rainbow trout. Journal of Neurophysiology, 114, 2703–2717.

Orger MB, & Baier H (2005). Channeling of red and green cone inputs to the zebrafish optomotor response. Visual Neuroscience, 22, 275–281 [PubMed: 16079003]

Perry RI, Stocker M, & Fargo J (1994). Environmental effects on the distributions of groundfish in Hecate Strait, British Columbia. Canadian Journal of Fisheries and Aquatic Sciences, 51, 1481–1409.

Pignatelli V, Champ C, Marshall J, & Vorobyev M (2010). Double cones are used for colour discrimination in the reef fish, Rhinecanthus aculeatus. Biology Letters, rsbl20091010.

Rau A, Lewin W-C, Zettler ML, Gogina M, & von Dorrien C (2019). Abiotic and biotic drivers of flatfish abundance within distinct demersal fish assemblages in a brackish ecosystem (western Baltic Sea). Estuarine, Coastal and Shelf Science, 220, 38–47.

Reckel F, Hoffman B, Melzer RR, Hoppila J, & Smola U (2003). Photoreceptors and cone patterns in the retina of the smelt Osmerus eperlanus (L.) (Osmeridae: Teleostei). Acta Zoologica, 84, 161–170.

Reckel F, & Melzer RR (2003). Regional variations in the outer retina of Atherinomorpha (Beloniformes, Atheriniformes, Cyprinodontiformes: Teleostei): Photoreceptors, cone patterns, and cone densities. Journal of Morphology, 257, 270–288. [PubMed: 12833370]

Reckel F, Melzer RR, & Smola U (2001). Outer retinal fine structure of the garfish Belone belone (L.) (Belonidae, Teleostei) during light and dark adaptation – photoreceptors, cone patterns and densities. Acta Zoologica, 82, 89–105.

Reese BE, & Keeley PW (2015). Design principles and developmental mechanisms underlying retinal mosaics. Biological Reviews, 90, 854–876. [PubMed: 25109780]

Reum JCP, & Essington TE (2011). Season- and depth-dependent variability of a demersal fish assemblage in a large fjord estuary (Puget Sound, Washington). Fishery Bulletin, 109, 186–197.

Rossi EA, & Roorda A (2010). The relationship between visual resolution and cone spacing in the human fovea. Nature Neuroscience, 13, 156–157. [PubMed: 20023654]

Ryer CH, Boersma KS, & Hurst TP (2012). Growth and distributional correlates of behavior in three co-occurring juvenile flatfishes. Marine Ecology Progress Series, 460, 183–193.

Ryer CH, Lemke JL, Boersma K, & Levas S (2008). Adaptive coloration, behavior and predation vulnerability in three juvenile north Pacific flatfishes. Journal of Experimental Marine Biology and Ecology, 359, 62–66.

Ryer CH, Stoner AW, & Titgen RH (2004). Behavioral mechanisms underlying the refuge value of benthic habitat structure for two flatfishes with differing anti-predator strategies. Marine Ecology Progress Series, 268, 231–243.

Savelli I, Novales Flamarique I, Iwanicki T, & Taylor JS (2018). Parallel opsin switches in multiple cone types of the starry flounder retina: Tuning visual pigment composition for a demersal life style. Scientific Reports, 8, 4763. [PubMed: 29555918]

Shand J, Archer MA, & Collin SP (1999). Ontogenetic changes in the cone photoreceptor mosaic in a fish, the black bream, *Acanthopagrus butcheri*. Journal of Comparative Neurology, 412, 203–217. [PubMed: 10441751]

Sobocinski KL, Ciannelli L,Wakefield WW, Yergey ME, & Johnson-Colegrove A (2018). Distribution and abundance of juvenile demersal fishes in relation to summer hypoxia and other environmental variables in coastal Oregon, USA. Estuarine, Coastal and Shelf Science, 205, 75–90.

Sohn D, Ciannelli L, & Duffy-Anderson JT (2016). Distribution of early life Pacific halibut and comparison with Greenland halibut in the eastern Bering Sea. Journal of Sea Research, 107, 31–42.

Suliman T, & Novales Flamarique I (2014). Visual pigments and opsin expression in the juveniles of three species of fish (rainbow trout, zebrafish, and killifish) following prolonged exposure to thyroid hormone or retinoic acid. Journal of Comparative Neurology, 522, 98–117. [PubMed: 23818308]

Takahashi Y, Hisatomi O, Sakabikara S, Tokunaga F, & Tsukahara Y (2001). Distribution of blue-sensitive photoreceptors in amphibian retinas. FEBS Letters, 501, 151–155. [PubMed: 11470275]

van der Meer HJ (1992). Constructional morphology of photoreceptor patterns in percomorph fish. Acta Biotheoretica, 40, 51–85.

van Hal R, van Kooten T, & Rijnsdorp AD (2016). Temperature induced changes in size dependent distributions of two boreal and three Lusitanian flatfish species: A comparative study. Journal of Sea Research, 107, 14–22.

Vinagre C, Fonseca V, Cabral H, & Costa MJ (2006). Habitat suitability index models for the juvenile soles, *Solea solea* and *Solea senegalensis*, in the Tagus estuary: Defining variables for species management. Fisheries Research, 82, 140–149.

Vinagre C, Maia A, Reis-Santos P, Costa MJ, & Cabral H (2009). Small-scale distribution of Solea solea and Solea senegalensis juveniles in the Tagus estuary (Portugal). Estuarine, Coastal and Shelf Science, 81, 296–300.

Vollen T, & Albert OT (2008). Pelagic behavior of adult Greenland halibut (Reinhardtius hippoglossoides). Fisheries Bulletin, 106, 457–470.

Wagner HJ (1990). Retinal structure of fishes In Douglas R and Djamgoz M (Ed.), The Visual System of Fish, (pp. 109–157). Springer.

Wagner HJ (1975). Comparative analysis of the patterns of receptor and horizontal cells in teleost fishes In Ali MA (Ed.), Vision in Fish (pp. 517–524). Plenum Press.

Wagner HJ, Fröhlich E, Negishi K, & Collin SP (1998). The eyes of deep-sea fish II. functional morphology of the retina. Progress in Retinal and Eye Research, 17, 637–685. [PubMed: 9777652]

Yeung C, & Yang M-S (2018). Spatial variation in habitat quality for juvenile flatfish in the southeastern Bering Sea and its implications for productivity in a warming ecosystem. Journal Sea Research, 139, 62–72.

Yokoyama S (2008). Evolution of dim-light and color vision pigments. Annual Review of Genomics and Human Genetics, 9, 259–282.

Yokoyama S (2000). Molecular evolution of vertebrate visual pigments. Progress in Retinal Eye Research, 19, 385–419. [PubMed: 10785616]

Zaunreiter M, Junger H & Kotrschal K (1991). Retinal morphology of cyprinid fishes: a quantitative histological study of ontogenetic changes and interspecific variation. Vision Research, 31, 383–394. [PubMed: 1843750]

Zukoshi R, Savelli I, & Novales Flamarique I (2018). Foraging performance of two fishes, the threespine stickleback and the Cumaná guppy, under different light backgrounds. Vision Research, 145, 31–38. [PubMed: 29678538]

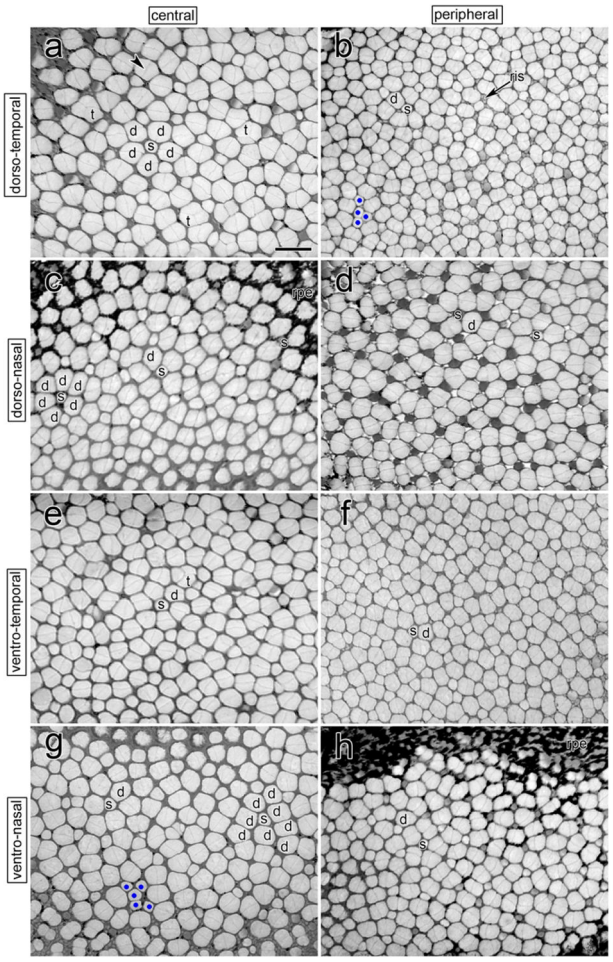

FIGURE 1.

Micrographs of tangential sections showing cone distributions at the level of largest ellipsoid cross section from various regions of the light adapted retina of the common sole. a: Central area from the dorso-temporal retina showing single (s), double (d), and triple (t) cones in various arrangements; the black arrowhead points to the partition linking two members of a double cone. b: Section from the dorso-temporal retina displaced further toward the periphery with respect to that shown in (a). The cones are smaller and rod inner segments (ris) are visible in between some cones. c,d: Central (c) and more peripheral (d) areas from the dorso-nasal retina. e,f: Central (e) and more peripheral (f) areas from ventro-temporal retina. g,h: Central (g) and more peripheral (h) areas from the ventro-nasal retina. Other abbreviations: rpe, retinal pigment epithelium. Blue dots indicate multiple groups of single cones. Scale bar = 10 μm in (a) applies to all panels.

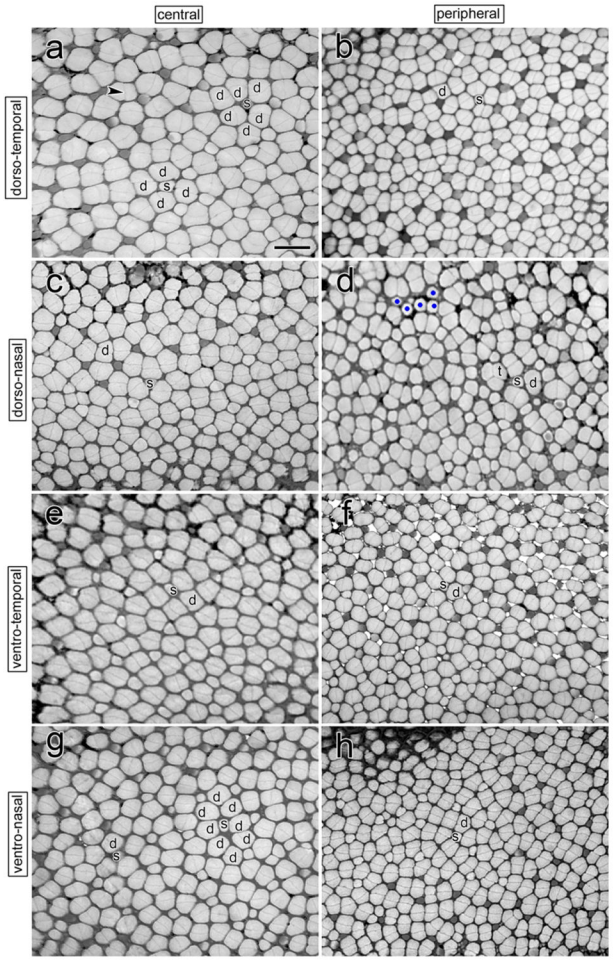

FIGURE 2.

Micrographs of tangential sections showing cone distributions at the level of largest ellipsoid cross section from various regions of the light adapted retina of the Senegalese sole. a,b: Central (a) and more peripheral (b) areas from the dorso-temporal retina. c,d: Central (c) and more peripheral (d) areas from the dorso-nasal retina. e,f: Central (e) and more peripheral (f) areas from ventro-temporal retina. g,h: Central (g) and more peripheral (h) areas from the ventro-nasal retina. Symbolism and abbreviations as per Figure 1. Scale bar = 10 μm in (a) applies to all panels.

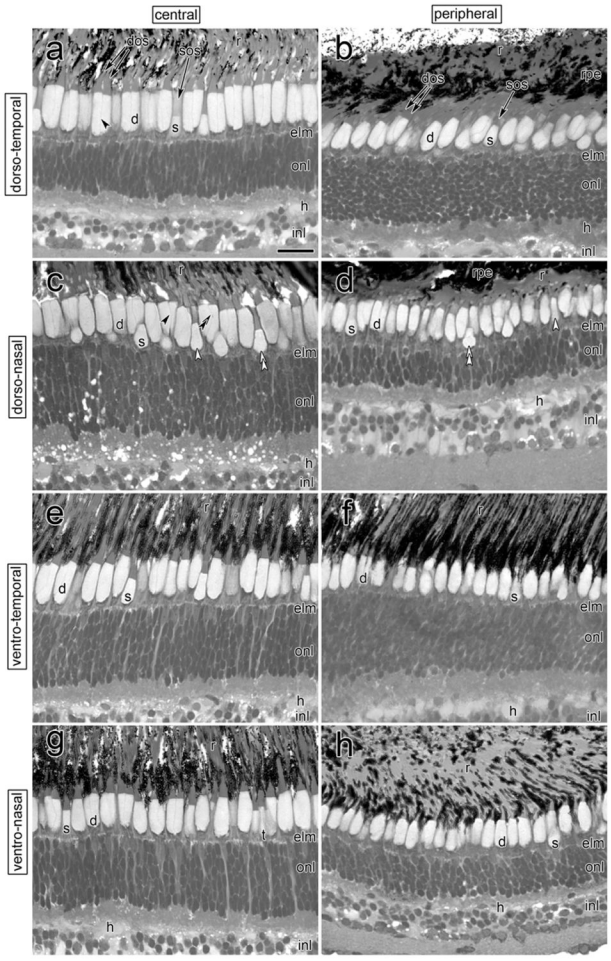

FIGURE 3.

Micrographs of radial sections showing cell layering from various regions representative of the light adapted retinas of the common sole and the Senegalese sole (sections from dorsal and ventral retina are from the common sole and the Senegalese sole, respectively). a: Central area from the dorso-temporal retina showing multiple double cones with straight partitions (black arrowhead) and a smaller number of single cones. The single cones have outer segments (sos) that are displaced vitreally with respect to those of the double cones (dos). The rod outer segments (r) are embedded within the retinal pigment epithelium. Abbreviations: elm, external limiting membrane; onl, outer nuclear layer; h, horizontal cell; inl, inner nuclear layer. b: Section from the dorso-temporal retina displaced further toward the periphery with respect to that shown in (a); the cones are smaller. c,d: Central (c) and more peripheral (d) areas from the dorso-nasal retina. These micrographs show the difference between double cones with a straight partition (black arrowhead) and those with a bent partition (double black arrowhead). Single cones could have a pear shaped inner segment (double white arrowhead) or be more elongated (white arrowhead). e,f: Central (e) and more peripheral (f) areas from ventro-temporal retina. g,h: Central (g) and more peripheral (h) areas from the ventro-nasal retina. A triple cone is visible in (g). Other abbreviations and nomenclature as in Figure 1. Scale bar = 10 μm in (a) applies to all panels.

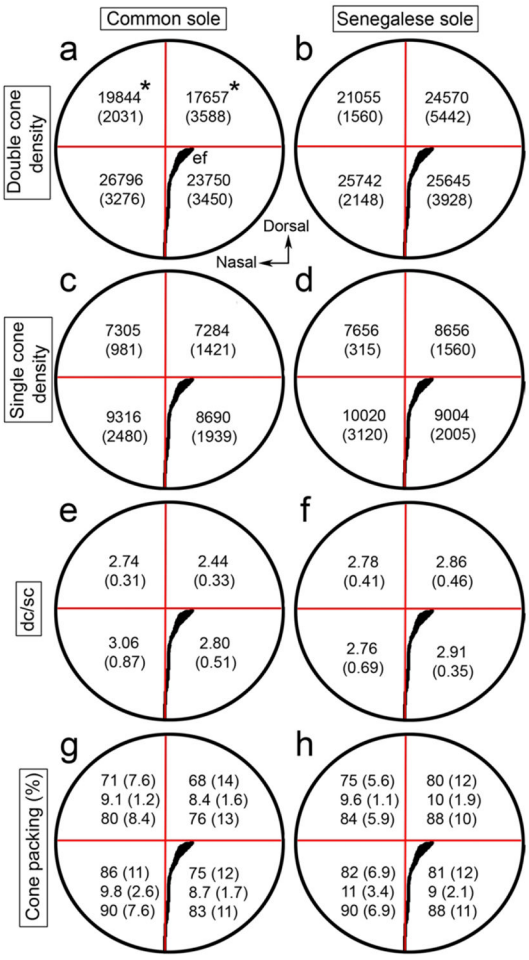

FIGURE 4.

Diagrams illustrating topographic maps of cone densities, double to single cone ratios, and cone packing from the retinas of eight fish per *Solea* species. Each number is the mean (± SD). a,b: Double cone density per mm^2 in the common sole (a) and the Senegalese sole (b). Asterisks (*) denote statistically equal means. c,d: Single cone density per mm^2 in the common sole (c) and the Senegalese sole (d). e,f: Double cone to single cone ratio (dc/sc) in the common sole (e) and the Senegalese sole (f). g,h: Packing (percentage of the retinal area occupied by a given cone type) for the double cone (top number), single cone (middle number) and for both cone types (bottom number) for the common sole (g) and the Senegalese sole (h). The embryonic fissure (ef) runs from the ventral retina toward the centro-temporal retina.

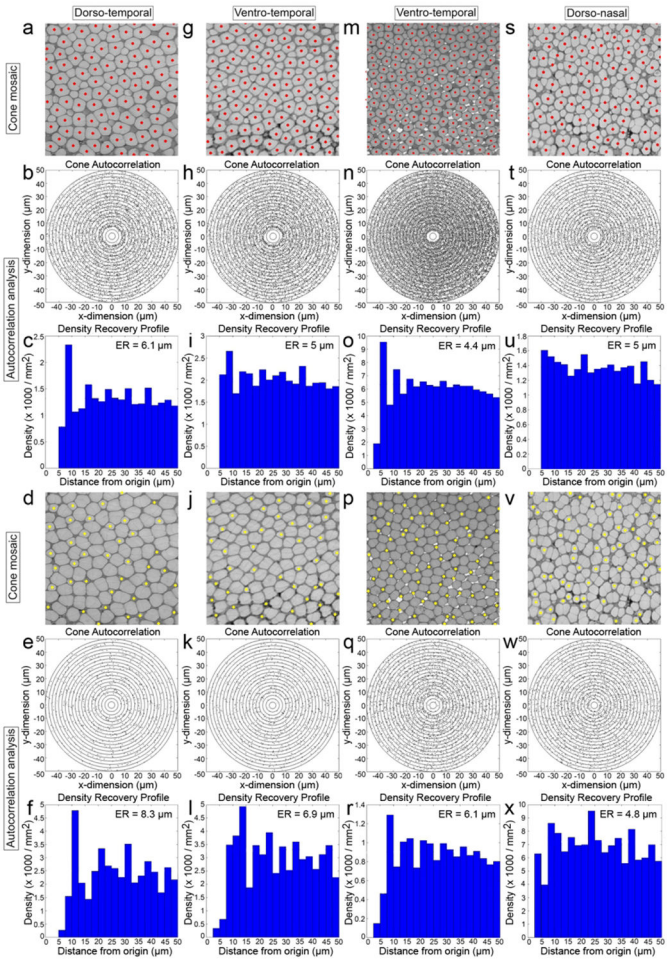

FIGURE 5.

Autocorrelogram (AC) and associated density recovery profile (DRP) for representative cone mosaics in the retina of the Senegalese sole (each field of view is 80 × 80 µm^2). a-c: Cone mosaic from the dorso-temporal retina with centroids of double cones (red dots) indicated (a), corresponding AC (b) and associated DRP (c) indicating the size of the null region at the centre of the AC, being the effective radius (ER). d-f: The same cone mosaic as in (a) but with the single cone centroids (yellow dots) indicated (d), corresponding AC (e) and associated DRP (f). g-l: Same presentation of data as per (a-f) but for the central ventro-temporal retina. m-r: Same presentation of data as per (a-f) but for more peripheral ventro-temporal retina. s-x: Same presentation of data as per (a-f) but for the more peripheral dorso-nasal retina. The mosaics shown in (a), (g), (m), and (s) correspond to regions within panels Figure 2 (a), (e), (f), and (d), respectively.

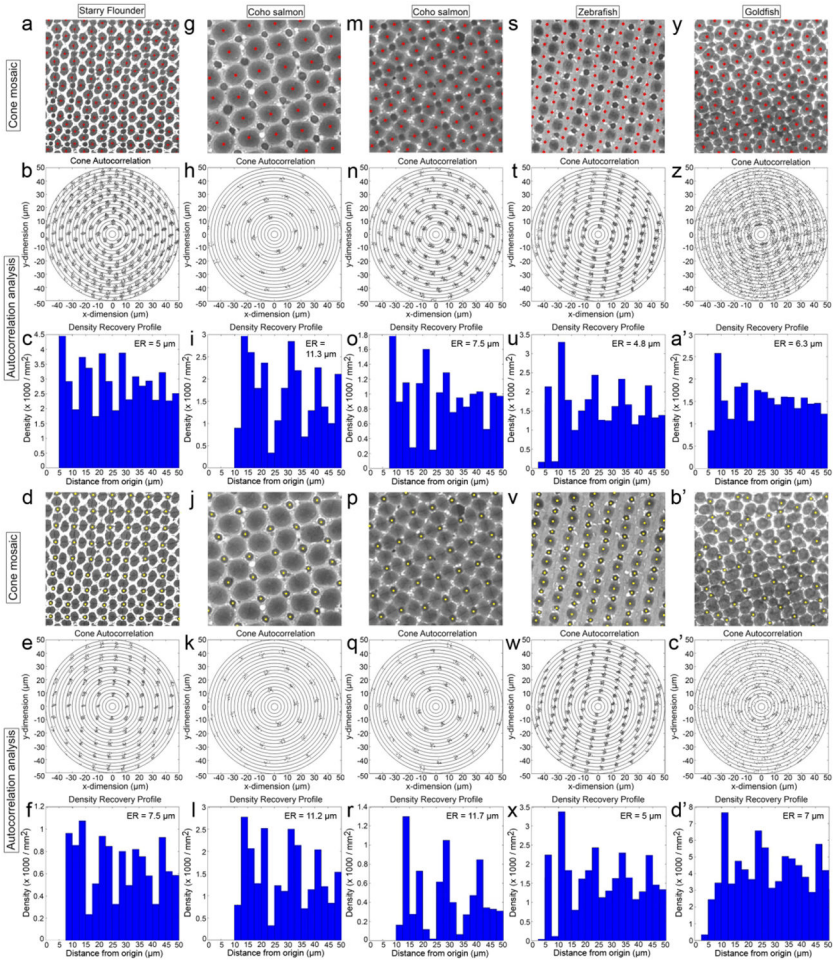

FIGURE 6.

AC and associated DRPs for representative cone mosaics in the retina of starry flounder, coho salmon, zebrafish, and goldfish (each field of view is 80 × 80 μm^2). a-c: Cone mosaic from the starry flounder retina with centroids of double cones (red dots) indicated (a), corresponding AC (b) and associated DRP (c) illustrating the size of the ER. d-f: The same cone mosaic as in (a) but with the single cone centroids (yellow dots) indicated (d), corresponding AC (e) and associated DRP (f). g-l: Same presentation of data as per (a-f) but for the dorsal retina of juvenile coho salmon (which has corner cones). m-r: Same presentation of data as per (a-f) but for the ventral retina of juvenile coho salmon (which does not have corner cones). s-x: Same presentation of data as per (a-f) but for the retina of zebrafish. y-d': Same presentation of data as per (a-f) but for the retina of juvenile goldfish.

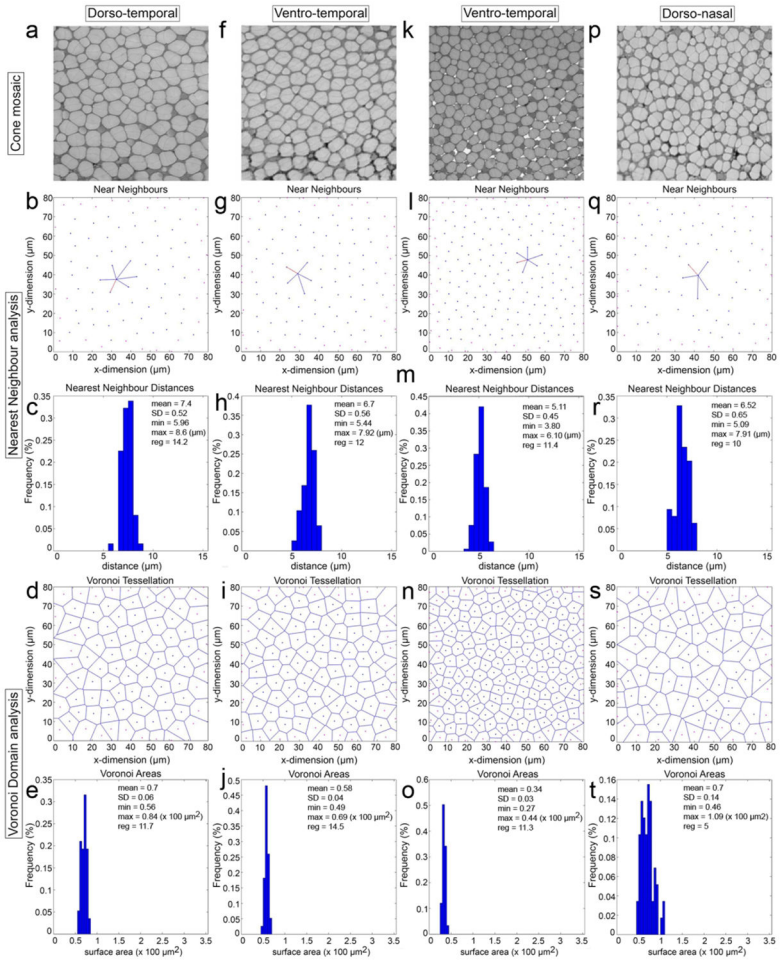

FIGURE 7.

Spatial analysis of double cone distributions from representative mosaics in the retina of the Senegalese sole (same mosaics as in Figure 5). a-e: Cone mosaic from the central dorso-temporal retina (a); Nearest neighbour analysis of double cone centroids, illustrating the near neighbours of a double cone (blue lines), including its nearest neighbour (red line) (b) and their frequency distribution (c) [statistics (in μm) are the mean nearest neighbour distance, its standard deviation (SD), the minimum (min) and maximum (max) nearest neighbour distances, and the regularity index (reg) = mean/SD]; Voronoi tessellation of double cone domains (d) and their frequency distribution (e) [statistics (in 100 μm^2) are the mean area (domain), its standard deviation (SD), the minimum (min) and maximum (max) areas, and the regularity index (mean/SD)]. f-j: Same presentation of data as per (a-e) but for the central ventro-temporal retina. k-o: Same presentation of data as per (a-e) but for more peripheral ventro-temporal retina. p-t: Same presentation of data as per (a-e) but for the more peripheral dorso-nasal retina. The blue and red dots in the centroid distribution and Voronoi domain diagrams indicate whether the data was included (blue) or not (red) in the statistical analysis. Exclusion occurs when a cell's nearest neighbour distance or Voronoi area cannot be accurately determined by virtue of being too close to the edge of the field.

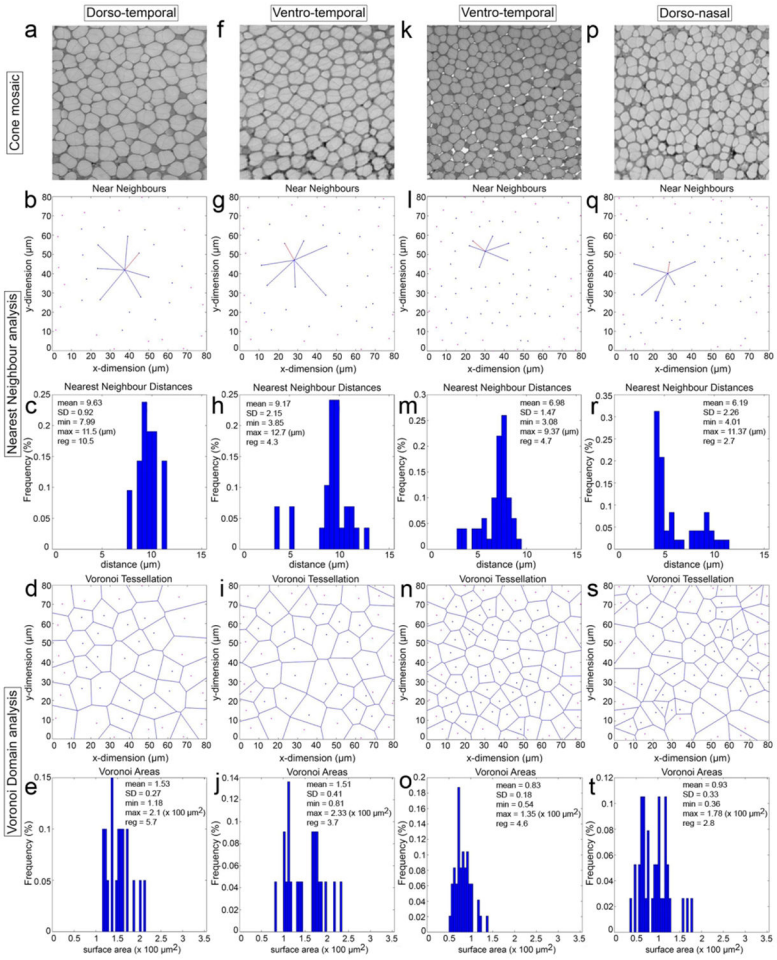

FIGURE 8.

Spatial analysis of single cone distributions from the same mosaics shown in Figure 7. Presentation of data as in Figure 7.

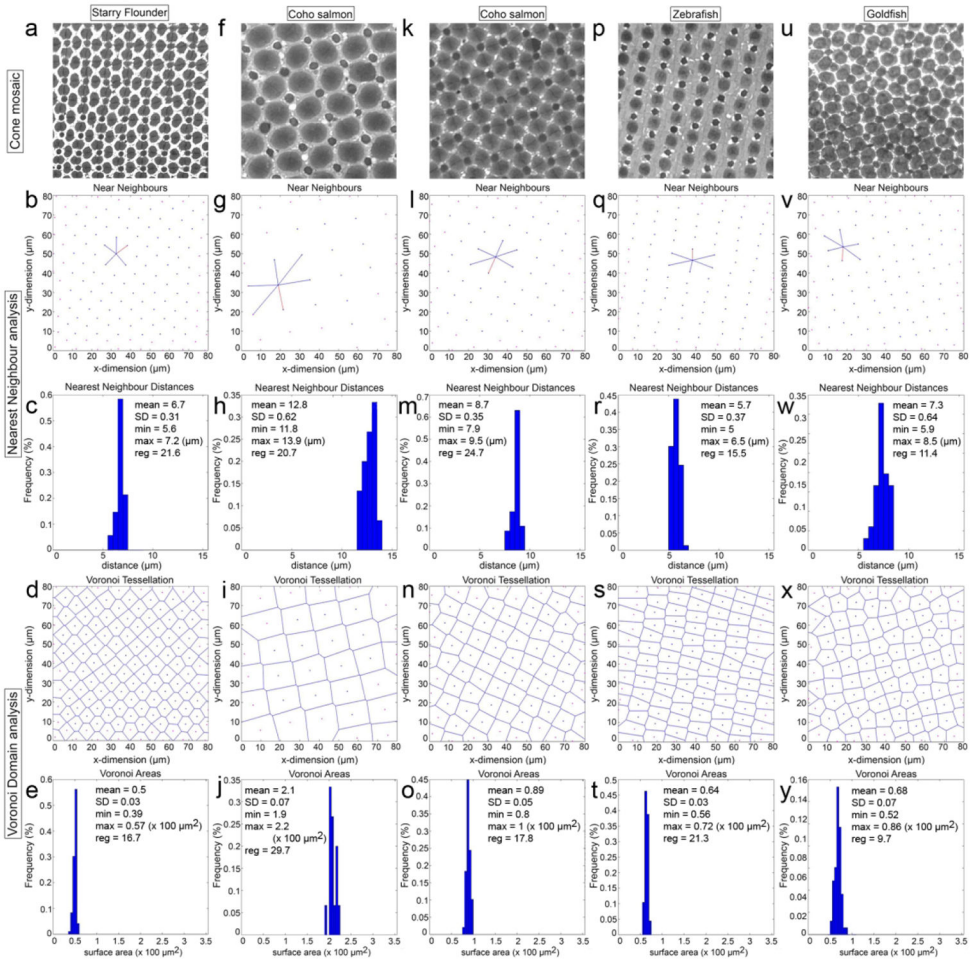

FIGURE 9.

Spatial analysis of double cone distributions from representative mosaics in the retina of starry flounder, coho salmon, zebrafish, and goldfish (same mosaics as in Figure 6). Presentation of data as in Figure 7.

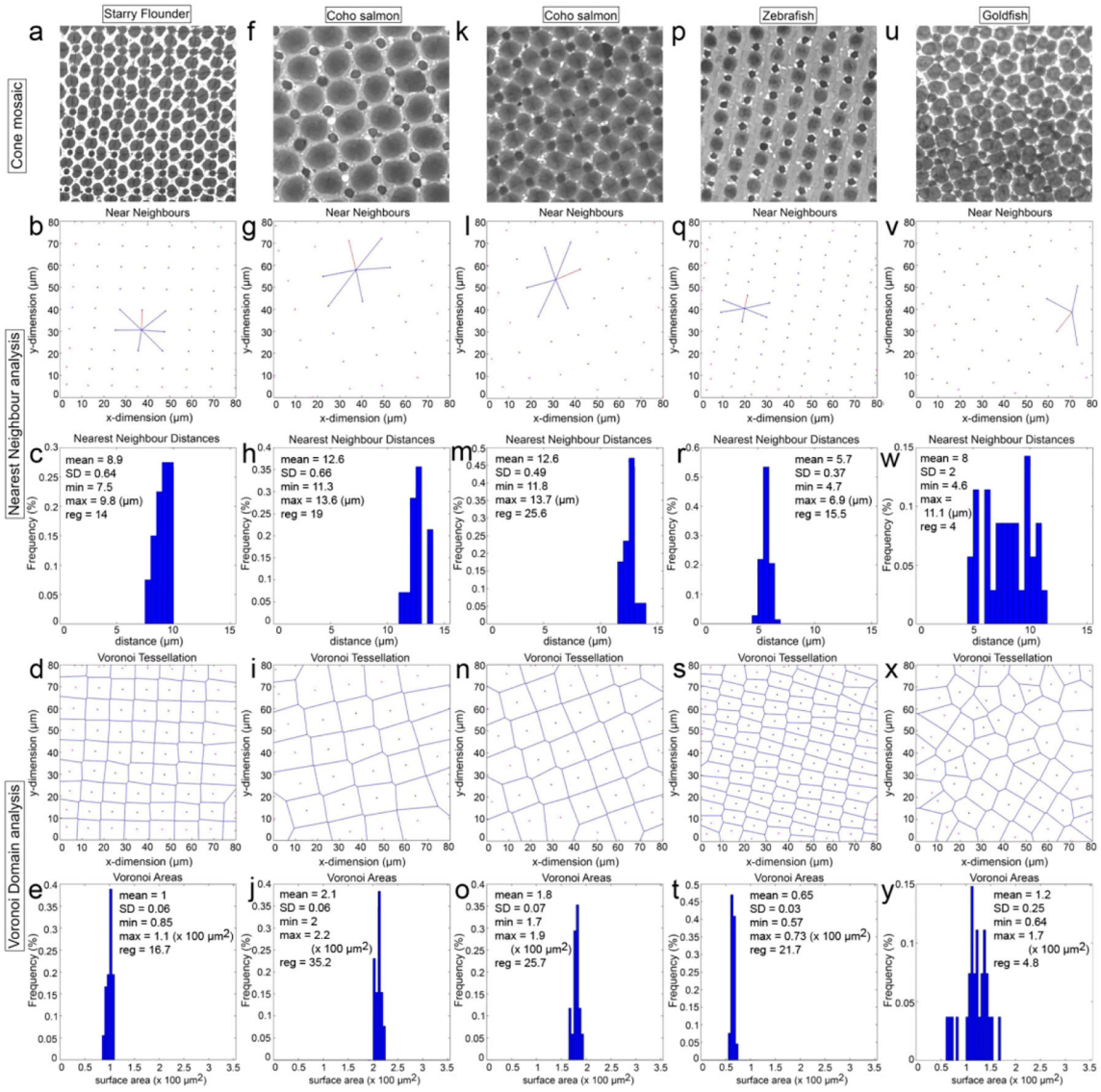

FIGURE 10.

Spatial analysis of single cone distributions from the same mosaics shown in Figure 9. Presentation of data as in Figure 9.

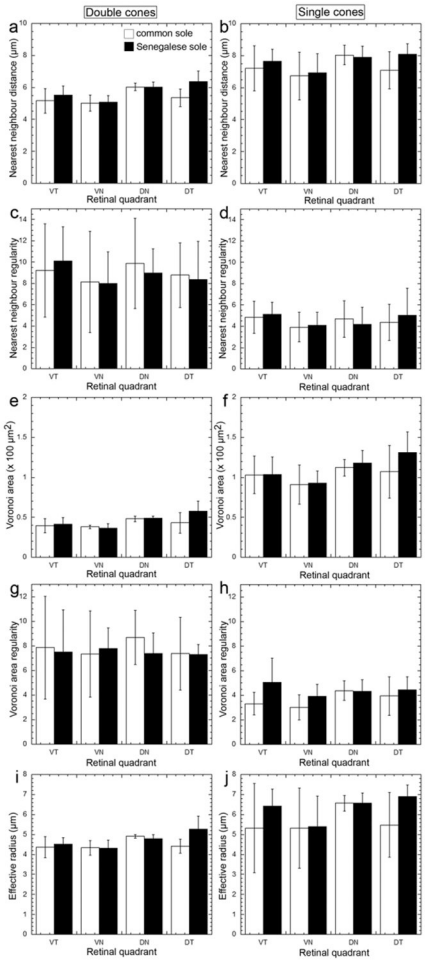

FIGURE 11:

Statistics (mean ± SD) of spatial analysis variables from the cone mosaics of eight retinas of the common sole and Senegalese sole, analyzed at mid-eccentricity, per quadrant. Abbreviations: VT, VN, DN, DT are the ventro-temporal, ventro-nasal, dorso-nasal, and dorso-temporal quadrants. These quadrants are depicted in Figure 4.

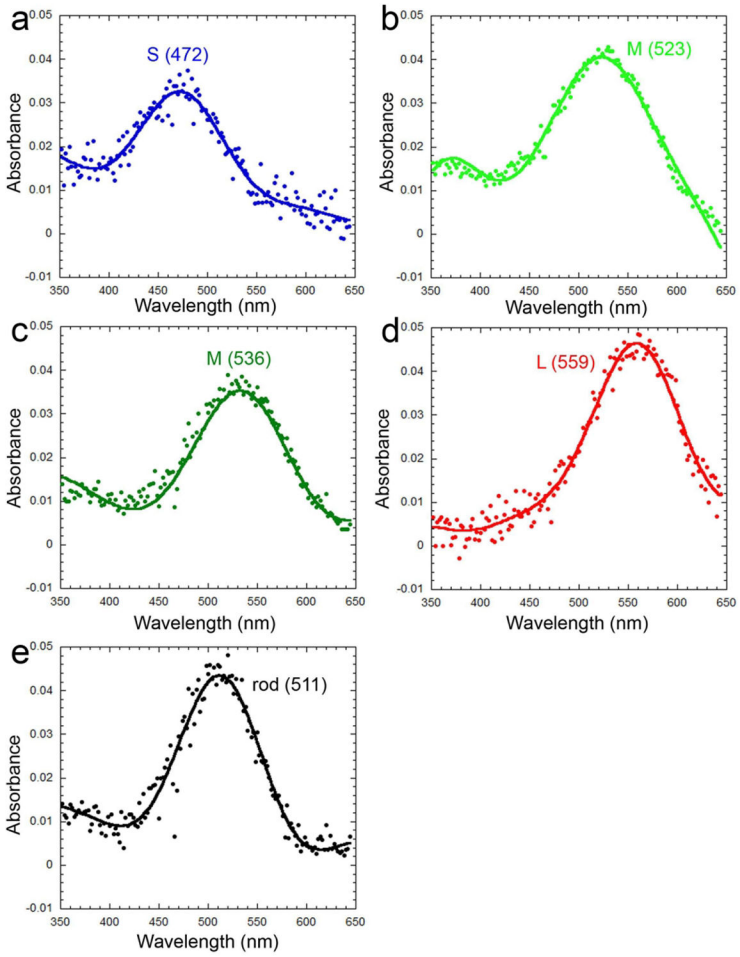

FIGURE 12.

Representative visual pigment absorbance spectra from isolated photoreceptors in common sole retina (each trace is the mean 5–16 records from 5 fish). a: Short wavelength sensitive [S (472)] visual pigment. b: Middle wavelength sensitive [M (523)] visual pigment. c: Middle wavelength sensitive [M (536)] visual pigment. d: Long wavelength sensitive [L(559)] visual pigment. e: Rod visual pigment [rod (511)]. The wavelength of maximum absorbance, λ_{max}, associated with each visual pigment type is in parenthesis.

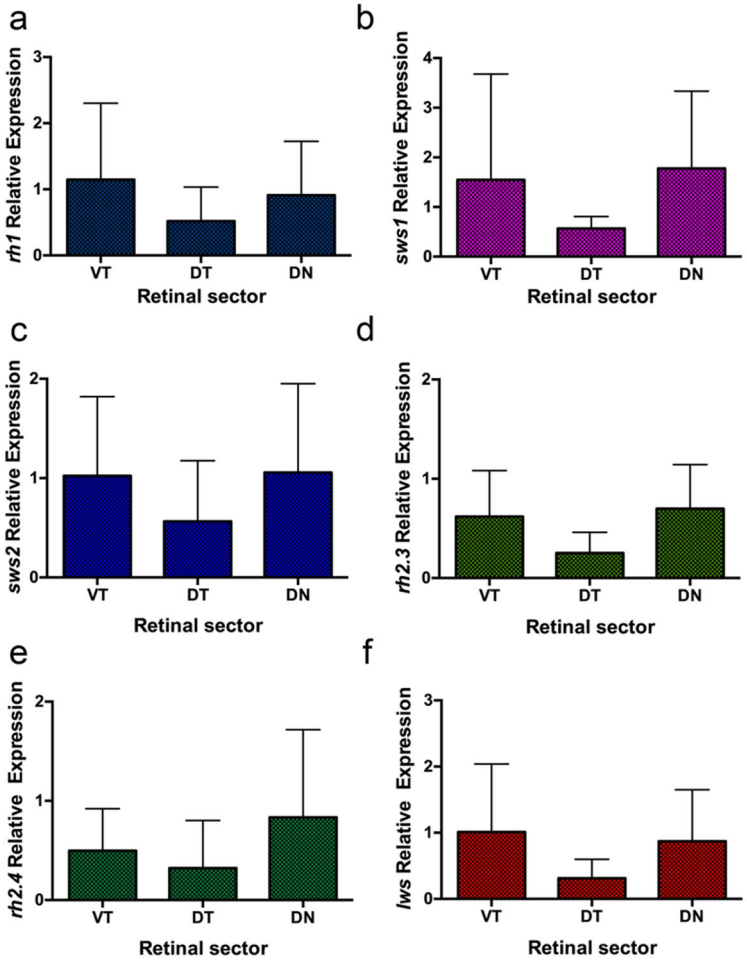

FIGURE 13.

Relative expression of opsin transcripts in the retina of the common sole. a-f: Mean relative transcript expression (± SD, n=8) of the VT, DT and DN quadrants with respect to the VN quadrant (calibrator) for *rh1* (a), *sws1* (b), *sws2* (c), *rh2.3* (d), *rh2.4* (e) and *lws* (f) opsins. All means within a given transcript type were not significantly different from each other ($p > 0.05$).

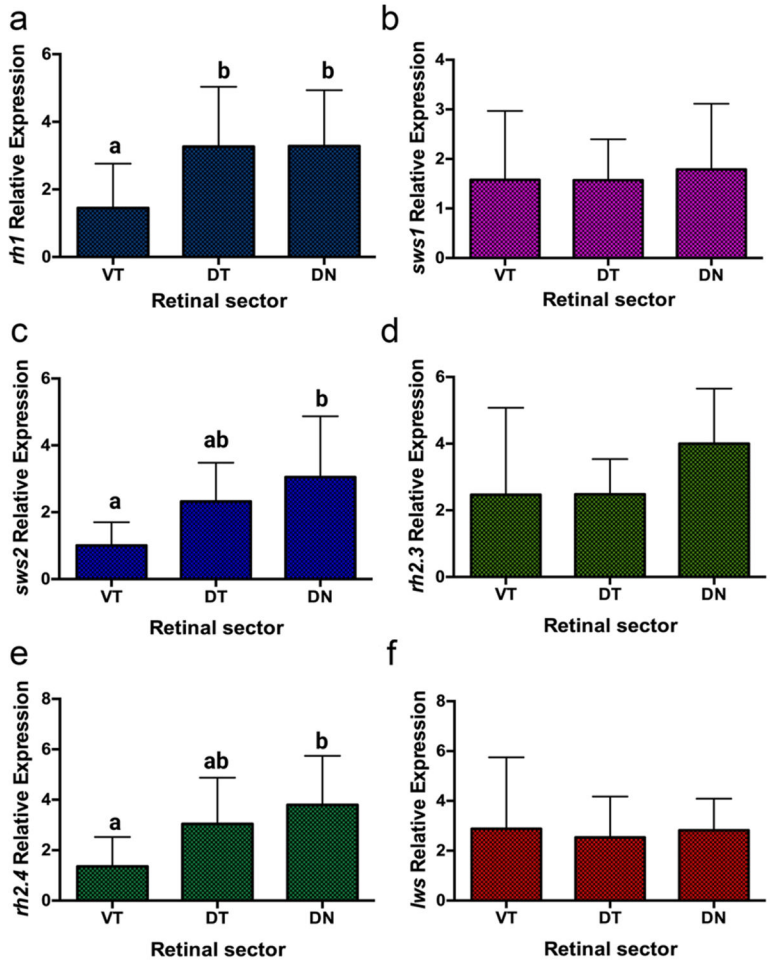

FIGURE 14.

Relative expression of opsin transcripts in the retina of the Senegalese sole. a-f: Mean relative transcript expression (± SD, n=10) of the VT, DT and DN quadrants with respect to the VN quadrant (calibrator) for *rh1* (a), *sws1* (b), *sws2* (c), *rh2.3* (d), *rh2.4* (e) and *lws* (f) opsins. For a given transcript type (i.e., within each panel), means that are unmarked or marked with the same letter are not significantly different from each other ($p > 0.05$).

TABLE 1.

Sequences of primers used for qPCR expression analysis of common sole visual opsins.

Gene	Oligo	Sequence (5’ to 3’)
Rh1	*Forward*	GAACACAAGAAGCTGCGAAC
Rh1	*Reverse*	CGACCAAGAACGAAGTAGC
Sws1	*Forward*	TCCCACCTTTCTTTGGTTGG
Sws1	*Reverse*	ACGTCACCATCAGGAAGTTG
Sws2	*Forward*	ATTGCATCACCTCCTCCACGT
Sws2	*Reverse*	CAGCAAAGCAGAAGCAGAAGAG
Rh2.3	*Forward*	ACAGTTTCGTAGCTGCATGC
Rh2.3	*Reverse*	TGAGGACACTTCTGTCTTGCTG
Rh2.4	*Forward*	ACACTTGGAGGTGAAGTTGC
Rh2.4	*Reverse*	TGGGTTTGCAGACACAATG
Lws	*Forward*	GAGACAGTTTTTGCCAGCAC
Lws	*Reverse*	AGACCACAGAGCAGCAATTC
18S	*Forward*	ACAGTTCAGCGCATGTGATG
18S	*Reverse*	ACAGCGACATGAAACAACCG

TABLE 2.

Sequences of primers used for qPCR expression analysis of Senegalese sole visual opsins.

Gene	Oligo	Sequence (5' to 3')
Rh1	*Forward*	CTACTTCGTTCTTGGTCGTCT
Rh1	*Reverse*	CGTAAAGCGGAAGTTGCTAATG
Sws1	*Forward*	TGCCATCCCACCTTTCTTT
Sws1	*Reverse*	GCTGCAGTGATACTCCTCATT
Sws2	*Forward*	TGCAAGATTGAAGGTTTTATGGC
Sws2	*Reverse*	CAAGTGGCTTACAGATGACCAG
Rh2.3	*Forward*	CAGAGGGCAAGAACTTCTACAT
Rh2.3	*Reverse*	GCTTCTTGTTCTGAGCTGTGAC
Rh2.4	*Forward*	TGAAGTTGCTCTCTGGTCTCTG
Rh2.4	*Reverse*	AGCCATGATCCAGGTGAAAGC
Lws	*Forward*	GGAATCAGAGTCAACCCAGAAA
Lws	*Reverse*	CCAGAGGATGGAAGGCATAAC
18S	*Forward*	GATTGACGGAAGGGCACCACCAG
18S	*Reverse*	ACTAAGAACGGCCATGCACCACCAC

TABLE 3.

Amino acid (a.a.) differences in opsin sequences between common sole and Senegalese sole when aligned to bovine rhodopsin. The asterisk (*) denotes a key tuning site position.

Gene	**Rh1**						**Sws1**												
a.a. position	19	124	165	213	217	277	58	97*	119	125	162	169	198	255	280	281	345	346	348
common sole	I	G	S	L	I	S	V	S	V	A	F	V	F	V	D	R	T	P	S
Senegalese sole	V	A	A	C	F	T	A	A	A	S	V	I	Y	I	E	P	S	T	V
Gene	**Sws2**																		
a.a. position	120	123	133	147	158	163	169	173	216	217	220	224	228	229	230	232	241	256	259
common sole	V	A	F	I	T	I	F	F	L	T	I	T	I	K	M	M	A	I	M
Senegalese sole	A	V	L	V	I	F	L	V	F	C	V	S	F	M	L	S	V	V	L
a.a. position	269*	276	292*	293	297	299	307	308	318	328	329	332	336	338	346				
common sole	A	S	A	V	S	A	I	V	L	G	D	E	Q	T	G				
Senegalese sole	T	T	S	C	A	T	V	I	M	V	E	T	T	A	E				
Gene	**Rh2.3**						**Rh2.4**												
a.a. position	25	49*	166	209	214	259	12	24	108	112	154	166	272	277	286	289			
common sole	D	C	S	V	L	I	I	Y	N	I	G	S	A	L	M	A			
Senegalese sole	E	S	A	I	F	L	V	F	T	V	A	A	T	M	L	S			
Gene	**Lws**																		
a.a. position	1	2	111	116*	172	205	249	259	290	324	332								
common sole	N	E	V	V	M	I	D	V	L	E	A								
Senegalese sole	H	D	I	I	I	V	E	L	M	Q	G								